NASA TECHNICAL NOTE

AERODYNAMIC CHARACTERISTICS OF A LARGE AIRCRAFT TO TRANSPORT SPACE SHUTTLE ORBITER OR OTHER EXTERNAL PAYLOADS

John W. Paulson, Jr.

Langley Research Center
Hampton, Va. 23665

NATIONAL AERONAUTICS AND SPACE ADMINISTRATION • WASHINGTON, D. C. • AUGUST 1975

1. Report No.	2. Government Accession No.	3. Recipient's Catalog No.
NASA TN D-7962		

4. Title and Subtitle	5. Report Date
AERODYNAMIC CHARACTERISTICS OF A LARGE AIRCRAFT TO TRANSPORT SPACE SHUTTLE ORBITER OR OTHER EXTERNAL PAYLOADS	August 1975
	6. Performing Organization Code

7. Author(s)	8. Performing Organization Report No.
John W. Paulson, Jr.	L-10065
	10. Work Unit No. 505-11-11-01

9. Performing Organization Name and Address	11. Contract or Grant No.
NASA Langley Research Center Hampton, Va. 23665	
	13. Type of Report and Period Covered Technical Note

12. Sponsoring Agency Name and Address	14. Sponsoring Agency Code
National Aeronautics and Space Administration Washington, D.C. 20546	

15. Supplementary Notes

16. Abstract

Wind-tunnel tests have been conducted in the Langley V/STOL tunnel to determine the aerodynamic characteristics of a large transport aircraft designed to carry the space shuttle orbiter or orbiter booster tank. Results indicate that the transport, with or without payloads, is statically stable, the longitudinal static margins being rather excessive. Elevator power is sufficient to trim the transport up to stall except when the orbiter is mounted close to the wing. Maximum lift-drag ratios at wind-tunnel Reynolds numbers vary from 12 to 14 depending on model configuration. Tests were conducted in the Langley V/STOL tunnel at Reynolds numbers from 1.21×10^6 to 1.49×10^6 with angle of attack from -2° to 20° and angle of sideslip from -5° to 5°.

17. Key Words (Suggested by Author(s))	18. Distribution Statement
Shuttle transport Large aircraft Stability and control Performance	Unclassified – Unlimited New Subject Category 08

19. Security Classif. (of this report)	20. Security Classif. (of this page)	21. No. of Pages	22. Price*
Unclassified	Unclassified	62	$4.25

*For sale by the National Technical Information Service, Springfield, Virginia 22161

AERODYNAMIC CHARACTERISTICS OF A LARGE AIRCRAFT TO TRANSPORT SPACE SHUTTLE ORBITER OR OTHER EXTERNAL PAYLOADS

John W. Paulson, Jr.
Langley Research Center

SUMMARY

A study has been conducted in the Langley V/STOL tunnel to investigate the aerodynamic characteristics of a large transport aircraft which was specifically designed to carry the space shuttle orbiter or the orbiter booster tank as external payloads. The static longitudinal and lateral-directional characteristics of the transport were determined with and without the orbiter and the booster tank payloads. The drag increments caused by the primary aircraft components were determined by a configuration buildup from the wing alone to the complete transport with the payloads. Data were obtained at angles of attack from -2° to 20° and angles of sideslip from -5° to 5°. Reynolds numbers based on wing mean geometric chord ranged from 1.21×10^6 to 1.49×10^6. These data indicate that the proposed transport aircraft will have acceptable lateral-directional stability with or without external payloads. However, the longitudinal stability is rather excessive with static margins of about 30 percent when the center of gravity is at the wing quarter chord. Elevator power is sufficient for trim over the lift coefficient range up to stall except when the orbiter is mounted close to the wing. Maximum trimmed lift-drag ratios at wind-tunnel Reynolds numbers are on the order of 12 to 14 depending on the model configuration. When extrapolated to flight Reynolds numbers, maximum lift-drag ratios are on the order of 15 to 18.

INTRODUCTION

Two of the mission requirements of the space shuttle program have led to the need for a large aircraft to carry the orbiter. The first mission is the atmospheric flight tests of the orbiter. The approach and landing phases of the flight tests require a system which can carry the orbiter to an altitude of 9100 m (30 000 ft) and release it for free flight. The second and much longer term mission is ferrying the orbiter or booster tank from the manufacturer or from a landing site to a launch site. For example, an orbiter returning from an orbital mission to Kennedy Space Center might need to be moved to the Vandenburg range 4000 km (2500 mile) away for the next orbital mission.

Since the orbiter cannot be flown on such a mission, a large aircraft is needed to transport the orbiter. It has been proposed that an existing B-747 aircraft be modified to meet these requirements. The B-747 would carry the orbiter or booster tank on top of the fuselage in piggyback fashion. (See ref. 1.) An alternative approach might be to develop a new aircraft for the mission requirements which could carry the orbiter below the aircraft rather than above as in the B-747 proposal. One configuration (ref. 2) for this new aircraft would use a high straight wing with a 137-m (450-ft) span and twin fuselages and tail booms. The orbiter or orbiter booster tank would be carried between the fuselages and below the high wing. (See figs. 1 and 2.)

An investigation was conducted in the Langley V/STOL tunnel to determine the static longitudinal and lateral-directional characteristics of the proposed transport with and without orbiter and booster tank payloads. The drag increments due to primary model components were determined and the orbiter position relative to the transport was investigated to determine a minimum drag configuration.

SYMBOLS

The data are presented in the stability-axis system as shown in figure 3. The model moment center was the quarter chord of the wing mean aerodynamic chord. All measurements and calculations were made in U.S. Customary Units; however, all values contained herein are given in both SI and U.S. Customary Units.

A	aspect ratio, b^2/S
b	wing span, m (ft)
c	local wing chord, m (ft)
$\bar{c}$	mean geometric chord, $\int c \, d\frac{y}{b/2}$, m (ft)
C_D	drag coefficient, $\frac{\text{Drag}}{qS}$
C_L	lift coefficient, $\frac{\text{Lift}}{qS}$
C_l	rolling-moment coefficient, $\frac{\text{Rolling moment}}{qSb}$
C_{l_β}	effective dihedral parameter based on increment of C_l between $\beta = -5^\circ$ and 5°, $\frac{\partial C_l}{\partial \beta}$

C_m pitching-moment coefficient, $\frac{\text{Pitching moment}}{qS\bar{c}}$

C_n yawing-moment coefficient, $\frac{\text{Yawing moment}}{qSb}$

C_{n_β} directional stability parameter based on increment of C_n between $\beta = -5^o$ and 5^o, $\frac{\partial C_n}{\partial \beta}$

C_Y side-force coefficient, $\frac{\text{Side force}}{qS}$

C_{Y_β} side-force parameter based on increment of C_Y between $\beta = -5^o$ and 5^o, $\frac{\partial C_Y}{\partial \beta}$

$h/\bar{c}$ height of orbiter pylon and mounting plate with respect to mean aerodynamic chord, measured from wing lower surface at quarter chord to top of orbiter or booster tank

i incidence of wing or horizontal tail, positive leading edge up, deg

L/D lift-drag ratio

q free-stream dynamic pressure, kN/m^2 (lbf/ft^2)

R Reynolds number based on $\bar{c}$

S area, m^2 (ft^2)

V velocity, m/sec (ft/sec)

x distance in x-direction (fig. 3), m (ft)

y distance in y-direction (fig. 3), m (ft)

α angle of attack of model reference line (tip chord), positive nose up (fig. 3), deg

β angle of sideslip of model reference line (center line of symmetry), positive nose left (fig. 3), deg

θ orbiter pitch angle relative to transport (angle between X-axis of model and X-axis of orbiter), deg

Subscripts:

max	maximum
t	horizontal tail
∞	free stream

APPARATUS AND PROCEDURES

The wind-tunnel model was a 0.0293-scale version of the proposed transport aircraft (ref. 2). Pertinent dimensions are given in table I and a three-view sketch is given in figure 4. The model wing had an aspect-ratio-8.98 rectangular planform with a 4.011-m (13.17-ft) span and an 0.445-m (1.46-ft) chord. The wing airfoil section was the 17-percent-thick GA(W)-1 (ref. 3) low-speed section and was constant across the span. The wing-root incidence was 2°, and the angle varied linearly to a tip incidence of 0°. The vertical and horizontal tails used the NACA 0012 airfoil section. The tail-boom cross sections were rectangular. The engine nacelles were existing 0.030-scale flowthrough nacelles which represented the external contours of the JT-9D engine.

The model, as tested, is somewhat different than the aircraft described in reference 2. The main difference is the lack of dihedral in the model wing, whereas the aircraft in reference 2 had 2° dihedral. The changes were made either to make use of available hardware (that is, an existing wing without dihedral) or to account for revisions suggested by the contractor.

Another significant difference was the mounting pylon for the transport payloads. The pylon tested is shown in figure 5. The large size and bulky shape of the pylon was due to model structural constraints. When the orbiter was mounted below the transport, the pylon had to carry all the loads from the transport to the balance mounted in the orbiter. This condition precluded using a small pylon similar to the aircraft mounting system and, as will be discussed later, the large pylon did cause some problems that were probably unique to the model tested.

Pylons were made for three vertical orbiter positions. The orbiter could be located at $h/\bar{c} = 0.37$, 0.26, and 0.14 (designated long, medium, and short pylons) distances below the wing and pitched $\pm 5^{\circ}$ relative to the transport. In addition, the pylons and mounting plate could be translated on the transport to locate the orbiter center of gravity at 0.20, 0.25, and 0.30 of the wing mean geometric chord.

TEST PROCEDURE

The following sequence was used for the transport component buildup (see fig. 4):

(1) The wing with internal balance was sting mounted in the test section.

(2) The tail booms were mounted to the wing spars.

(3) The body pylons were attached to the bottom of the tail booms.

(4) The fuselages were attached to the bottom of the body pylons.

(5) The engine nacelles were pylon mounted to the wing leading edge.

(6) The vertical tails were mounted to the upper side of the tail booms.

(7) The horizontal tail was mounted between the two vertical tails.

(8) The mounting plate and pylon were attached to the lower surface of the wing.

Static longitudinal and lateral-directional data were obtained for each of the configurations listed. When the transport buildup was complete, the horizontal-tail incidence was varied from 0° to -5° to -10°. As will be discussed, it was found that a tail incidence of -5° trimmed the transport near the wing design lift coefficient; therefore, except when the tail incidence was varied to obtain trim data, all runs were made with $i_t = -5^{\circ}$.

Data were obtained with payloads mounted on the transport. The first payload was an 0.0293-scale shuttle orbiter model. The orbiter-transport combination was sting mounted with the balance located inside the orbiter. The balance could not be located in the transport as was done in the transport tests because the tail of the orbiter blocked access to the balance housing area in the transport. With the balance in the orbiter, the mounting plate and pylon actually mounted the transport to the top of the orbiter. These two sting positions can be seen in figures 1 and 2(a).

The static longitudinal and lateral-directional characteristics were obtained at each vertical orbiter location with and without an orbiter tail fairing. The longitudinal data were obtained with horizontal tail off and with horizontal tail on for tail incidences of 0°, -5°, -10°, and -15°.

In addition to the orbiter, an 0.0293-scale orbiter booster tank was constructed and mounted between the transport fuselages. The tank was mounted on a pylon so that $h/\bar{c} = 0.20$ and the tank center of gravity was $x/\bar{c} = 0.25$. Since there was no vertical tail on the booster tank, the sting was mounted in the transport wing. (See fig. 2(b).)

Finally, there were several runs made to obtain data on the effect of pitching the orbiter $\pm 5^{\circ}$ as well as moving the orbiter center of gravity to $x/\bar{c} = 0.20$ and $x/\bar{c} = 0.30$.

These tests were conducted in the Langley V/STOL tunnel. The Reynolds numbers, based on mean geometric chord, were 1.21×10^6 and 1.49×10^6. These values corresponded to dynamic pressures of 0.95 kN/m^2 (20 lbf/ft^2) and 1.44 kN/m^2 (30 lbf/ft^2). Most testing was done at the higher dynamic pressure. In several instances, the balance limits would have been exceeded; thus, a lower dynamic pressure was dictated. The Reynolds number effects associated with changing the dynamic pressure were negligible. Angle of attack ranged from -2° to 20° and sideslip angle ranged from -5° to 5°. All measurements were made electronically. Forces and moments were measured with an internal six-component strain-gage balance. Angle of attack was measured with an accelerometer mounted inside the model. Sideslip angle was measured from the sting-support system position. Transition (grit size 60) was fixed near the leading edge of each model component (see ref. 4) as shown in the following table:

Model component	Transition strip location streamwise from leading edge, cm (in.)
Wing	2.23 (0.88); upper surface 4.32 (1.70); lower surface
Horizontal tail	2.23 (0.88)
Vertical tail	2.23 (0.88)
Body pylon	5.08 (2.00)
Fuselages	5.08 (2.00)
Tail booms and engine nacelles	No fixed transition

All data were corrected for jet-boundary effects according to reference 5. No other corrections were made to the data.

PRESENTATION OF RESULTS

The results of this investigation have been reduced to coefficient form and are presented as follows:

DISCUSSION

The discussion of results is separated into two main sections: the static characteristics of the transport alone and the static characteristics of the transport with payloads.

Transport Characteristics

Transport component buildup.- The model buildup from the wing alone to the complete transport is presented in figure 6. The drag coefficient level for the wing alone at the design cruise lift coefficient $(C_L = 0.40)$ (ref. 3) was 0.022. The drag coefficient for the transport without the horizontal tail at $C_L = 0.40$ was 0.033. Therefore, the drag increment due to all model components except the horizontal tail is $\Delta C_D = 0.011$, and this increment is almost constant up to $C_L = 1.0$. Above this lift coefficient, increases in ΔC_D are probably due to flow-separation effects on the model components. Throughout the C_L range (0.15 to 1.0), well over half of the drag increment is caused by the tail booms and body pylons. The horizontal tail with an incidence of -5° trims the transport at $C_L = 0.44$ and adds an additional drag increment of 0.0045 which is nearly constant from $C_L = 0.40$ to $C_L = 0.65$. At $C_L = 0.44$ the trimmed transport has a C_D of 0.038; this value is a total increase of 0.016 over the wing alone at this C_L. The component buildup causes a reduction in lift, generally between $\Delta C_L = -0.05$ to -0.1 over the entire C_L range and a negligible change in pitching moment for the tail-off configuration. (See fig. 6(a).) The horizontal tail provides a stability level of $\partial C_m/\partial C_L = -0.33$ for a transport center-of-gravity location of $x/\bar{c} = 0.25$. The model center of gravity must be moved to $x/\bar{c} = 0.53$ if a desirable stability level of $\partial C_m/\partial C_L = -0.05$ is to be obtained. This stability level could also be obtained by reducing the horizontal tail volume.

Longitudinal control characteristics.- Longitudinal characteristics for the transport alone with tail incidences of 0°, -5°, and -10° are given in figure 7. The static longitudinal stability of the transport at the trim points is between 30 percent and 35 percent, depending on the tail incidence. As discussed, these static margins are excessive and would have to be reduced for a flight vehicle.

Trimmed L/D curves and drag polars are given in figure 19. At the design C_L, the trimmed C_D is 0.038 and the maximum L/D of 14.0 occurs at $C_L = 0.80$. The data were extrapolated to flight Reynolds number and are discussed later.

Lateral-directional characteristics of transport.- The static lateral-directional characteristics for the transport component buildup are presented in figure 8 and the stability derivatives are given in figure 9. The wing alone shows approximately neutral static lateral and directional stability at $\alpha = 0^{\circ}$. Although the tail booms add to the directional and lateral stability, the body pylons, fuselages and nacelles are all directionally destabilizing. The model without a vertical tail is slightly directionally unstable up to $\alpha = 14^{\circ}$ and slightly laterally stable up to $\alpha = 14^{\circ}$. As expected, the vertical tail provides the transport model with directional stability throughout the angle-of-attack range of 0° to 14°. The levels of stability are adequate for angles of attack up to stall. In addition, the side force due to sideslip exhibited no unusual characteristics.

Transport Characteristics With Payloads

Transport with orbiter payload.- Effect of payload mount: The effect of adding the mounting plate and mounting pylon to the transport is presented in figure 10. The orbiter is attached to the pylon and transport in figure 11. The transport at $C_L = 0.44$ has a C_D of 0.043 when the long ($h/\bar{c} = 0.37$) mounting pylon is installed and a C_D of 0.0405 when the mounting plate alone is installed. The transport alone has a drag coefficient of 0.038; thus, the mounting plate and long pylon cause drag increments of 0.002 and 0.005, respectively. At the cruise C_L, this increase is about equal to the drag increment due to the entire orbiter. (See fig. 7.) The total drag increment for the orbiter and long pylon is 0.008 with 0.005 of this attributed to the pylon alone. Similarly, the drag increment for the orbiter and short ($h/\bar{c} = 0.14$) pylon is 0.006 with 0.002 of this value attributed to the pylon. In fact, at the higher lift coefficients, the mounting pylon causes more drag than does the orbiter-pylon combination. This condition may be accounted for by noting that the drag increments are largest where there is a corresponding break in the pitching-moment curve; it appears that there may be a wake from the pylon area that impinges on the horizontal tail and causes some local flow variations that result in higher drag and an increase in tail effectiveness.

As discussed before, the mounting plate and mounting pylon were designed for structural constraints rather than for aerodynamic efficiency; therefore, the resulting wake and high drag increments are probably unique to the configuration.

Effect of orbiter tail fairing: The effect of adding an orbiter tail fairing is presented in figure 12. The tail fairing has almost no effect on lift or pitching moment but it does reduce the drag increments for the orbiter. With the tail fairing the drag of the transport and orbiter combination is reduced to 0.046 for the long pylon and to 0.044 for the short pylon. The fairing therefore reduces the drag by about 0.002 which reduces the drag increment due to the orbiter by about 1/3.

Effect of orbiter position: The orbiter was tested at several positions beneath the wing. These positions included three vertical positions of the orbiter relative to the transport ($h/\bar{c}$ = 0.14, 0.26, and 0.37) with the orbiter center of gravity at $x/\bar{c}$ = 0.25 and $\theta = 0^{o}$ (figs. 13 and 14); three longitudinal positions of orbiter center of gravity ($x/\bar{c}$ = 0.20, 0.25, and 0.30) with $h/\bar{c}$ = 0.37 and $\theta = 0^{o}$ (fig. 13); and three pitch angles of the orbiter relative to transport ($\theta = -5^{o}$, 0^{o}, and 5^{o}) with $h/\bar{c}$ = 0.37 and orbiter center of gravity at $x/\bar{c}$ = 0.25. (See fig. 16.)

The lowest drag occurs when $h/\bar{c}$ = 0.14 and the tail fairing is on the orbiter. (See fig. 13.) At a C_L of 0.44, C_D = 0.460 when the orbiter is mounted on the long pylon and this value is reduced to C_D = 0.440 when the short pylon is used. The latter orbiter position also gives the highest C_L for a given angle of attack below stall. The orbiter decreases the static stability by about 5 percent from the transport alone value. The lift and pitching moment of the orbiter causes the trimmed C_L of the transport to vary slightly as the orbiter position changes. Since the drag increments are basically constant over the lower C_L range, all comparisons were made at C_L = 0.44 rather than at each trim point. Although the same trends are present when the orbiter tail fairing is removed (fig. 14), the drag reduction due to pylon height variation is only about 1/2 to 1/3 the reduction obtained when the tail fairing is used.

Variation in longitudinal location of the orbiter with the long pylon (fig. 15) has a negligible effect on lift, a small effect on the longitudinal stability, and causes a small reduction in drag when the orbiter is located away from $x/\bar{c}$ = 0.25. The drag is about the same for orbiter locations at $x/\bar{c}$ = 0.20 or $x/\bar{c}$ = 0.30.

Pitching the orbiter nose up 5^{o} relative to the transport on the long pylon (fig. 16) causes a sizable increase in lift and a decrease in static longitudinal stability but it also slightly increases the drag. Pitching the orbiter nose downward -5^{o} has very little effect on lift and increases the static longitudinal stability but reduces the drag. Drag levels for the nose-downward case are reduced about 0.004 to 0.005 over the cruise lift coefficient range. In addition, the static longitudinal stability is increased about 5 percent when the orbiter is pitched 5^{o} nose downward.

Since there were no data taken with the orbiter pitched or moved longitudinally at the other pylon heights, an optimum configuration cannot be defined. However. if the effect of orbiter pitch and longitudinal location were to remain the same when the orbiter is positioned close to the transport, a better configuration would be obtained with the orbiter at $h/\bar{c}$ = 0.14, center of gravity at $x/\bar{c}$ = 0.30, and pitched nose downward -5^{o}.

Transport with booster tank payload.- The results of the transport with orbiter booster tank (fig. 17) show longitudinal stability on the order of $\partial C_m/\partial C_L$ = -0.30 and C_L and C_D levels similar to the transport with the orbiter. No attempt was made to optimize this configuration by varying the position of booster tail relative to the transport.

Longitudinal control characteristics.- Longitudinal control characteristics for the transport and orbiter combination are presented in figure 18. Tail incidences ranged from 0^{o} to -15^{o} for the orbiter on the long and short pylons. However, for the middle pylon tests were only for $i_t = -5^{o}$. It is seen in figure 14 that decreasing the mounting pylon length decreases static stability; however, these levels are still considerably above the desired static margin of 5 percent. The trim lift coefficients remain fairly constant as the orbiter and transport separation is decreased for tail incidences of 0^{o}, -5^{o}, or -10^{o}. Although a tail incidence of -15^{o} will trim the configuration with the orbiter on the long pylon all the way up to a $(C_L)_{max}$ of 1.38, it will only trim the configuration with the orbiter on the short pylon up to a C_L of 1.2. The tail at -15^{o} incidence is apparently losing effectiveness in the wake of the orbiter on the short pylon.

The data presented in figures 7 and 18 were used to construct the trimmed L/D curves and drag polars of figure 19. As discussed before at the design $C_L = 0.40$, the trimmed C_D of the transport is 0.038. The trimmed C_D for the transport with orbiter on the long pylon and short pylon are 0.047 and 0.044, respectively, and these pylons give drag increments of approximately 0.009 and 0.006. The maximum lift-drag ratio is 11.7 and 12.4 for each configuration and occurs at a common lift coefficient of 0.8. As in the untrimmed condition the transport has lower drag when the transport-orbiter separation distance is reduced.

Extrapolation of Data to Flight Reynolds Number

The data for transport with and without payloads were extrapolated to a flight Reynolds number corresponding to a cruise condition of 300 knots at 9144 m (30 000 ft) on a standard day. The data were extrapolated by correcting the skin-friction coefficient of the model for Reynolds number effects by use of a Langley computer program. This program uses the Kármán-Schoenherr skin-friction law (ref. 6) and the Sommer and Short compressibility correction (ref. 7) to predict the skin-friction coefficient of an aircraft. The skin-friction coefficient of the model at wind-tunnel Reynolds number was computed and subtracted out of the wind-tunnel drag data. The skin-friction coefficient at flight Reynolds number was then computed and added back into the wind-tunnel data to give a corrected C_D. There was no attempt to correct for roughness or interference drag. The extrapolated data indicate the $(L/D)_{max}$ is about 18.0 for the transport and about 15.5 for the transport with orbiter or the short pylon. (See fig. 19.)

Lateral-directional characteristics.- The lateral-directional characteristics for the transport with orbiter, with and without the orbiter tail fairing, are presented in figures 20 and 21, respectively. The stability derivatives for the transport with orbiter, with tail fairing, on the long and short pylon are presented in figure 22. The orbiter has

a small stabilizing effect on the static lateral characteristics. The orbiter also has a slight stabilizing effect on the directional stability at angles of attack less than 6^{o}. Above 6^{o} the orbiter decreases the directional stability although it is still thought to be acceptable.

Transport with booster tank payload.- Figure 23 shows the lateral-directional characteristics for the transport with orbiter booster tank. This configuration has stability characteristics similar to those for the transport and orbiter.

SUMMARY OF RESULTS

An investigation has been conducted to determine the aerodynamic characteristics of a large transport aircraft which was designed to carry either the space shuttle orbiter or the shuttle booster tank. The results show the following aircraft characteristics:

1. The transport with and without payloads is statically stable both longitudinally and lateral directionally. The static lateral directional stability appears to be acceptable whereas the static longitudinal stability of 30 percent is excessive.

2. The orbiter drag increment is reduced when the separation height of the transport and orbiter is reduced. Also the increment is reduced if the orbiter is pitched slightly nose downward or moved longitudinally to 0.30 wing chord.

3. Elevator power is sufficient to trim the transport with orbiter payload up to the maximum lift coefficient $(C_L)_{max}$ except when the orbiter is mounted on the short pylon.

4. The transport alone has a trimmed maximum lift-drag ratio $(L/D)_{max}$ of 14.0 at wind-tunnel Reynolds number and 18.0 at full-scale Reynolds number. These values are reduced to around 12.0 and 14.6, respectively, when the orbiter is mounted to the transport.

5. The transport with booster tank payload has characteristics similar to those of the transport with orbiter payload in that there are no apparent performance or control problems.

Langley Research Center,
National Aeronautics and Space Administration,
Hampton, Va., May 5, 1975.

REFERENCES

1. Fink, Donald E.: Shuttle Orbiter Flight Test Plan Evolves. Aviat. Week & Space Technol., vol. 101, no. 19, Nov. 11, 1974, pp. 45-47, 49.

2. Giant Aircraft Would Lift Shuttle Orbiter. Aviat. Week & Space Technol., vol. 100, no. 5, Feb. 4, 1974, pp. 38-39, 41.

3. McGhee, Robert J.; and Beasley, William D.: Low-Speed Aerodynamic Characteristics of a 17-Percent Thick Airfoil Section Designed for General Aviation Applications. NASA TN D-7428, 1973.

4. Braslow, Albert L.; and Knox, Eugene C.: Simplified Method for Determination of Critical Height of Distributed Roughness Particles for Boundary-Layer Transition at Mach Numbers From 0 to 5. NACA TN 4363, 1958.

5. Gillis, Clarence L.; Polhamus, Edward C.; and Gray, Joseph L., Jr.: Charts for Determining Jet-Boundary Corrections for Complete Models in 7- by 10-Foot Closed Rectangular Wind Tunnels. NACA WR L-123, 1945. (Formerly NACA ARR L5G31.)

6. Schoenherr, Karl E.: Resistance of Flat Surfaces Moving Through a Fluid. Trans. Soc. Naval Architects Marine Eng., vol. 40, 1932, pp. 279-313.

7. Sommer, Simon C.; and Short, Barbara J.: Free-Flight Measurements of Turbulent-Boundary-Layer Skin Friction in the Presence of Severe Aerodynamic Heating at Mach Numbers From 2.8 to 7.0. NACA TN 3391, 1955.

TABLE I.- DIMENSIONS FOR TRANSPORT AND SHUTTLE ORBITER

(a) Transport

Body length:	
Overall, m (ft)	2.450 (8.039)
Fuselage, m (ft)	1.290 (4.233)
Wing:	
Span, m (ft)	4.013 (13.167)
Chord, m (ft)	0.447 (1.467)
Area, m^2 (ft^2)	1.7940 (19.311)
Aspect ratio	8.98
Twist	2^o washout
Section	Tip, GA(W)-1: root, GA(W)-1
Horizontal tail:	
Span, m (ft)	0.893 (2.93)
Chord, m (ft)	0.448 (1.47)
Area, m^2 (ft^2)	0.400 (4.307)
Tail length, m (ft)	1.27 (4.18)
Aspect ratio	1.99
Section	NACA 0012
Vertical tail:	
Span, m (ft)	0.429 (1.408)
Chord:	
Tip, m (ft)	0.175 (0.575)
Root, m (ft)	0.540 (1.773)
Area:	
Each, m^2 (ft^2)	0.162 (1.744)
Total, m^2 (ft^2)	0.324 (3.488)
Section:	
Tip	NACA 0012
Root	NACA 0012
Distance between fuselages, m (ft)	0.893 (2.93)

(b) Orbiter

Length:	
Overall, m (ft)	1.097 (3.598)
Body, m (ft)	0.960 (3.150)
Wing:	
Span, m (ft)	0.697 (2.287)
Chord:	
Tip, m (ft)	0.102 (0.336)
Root, m (ft)	0.513 (1.683)
Mean, m (ft)	0.353 (1.159)
Area, m^2 (ft^2)	0.21450 (2.309)
Aspect ratio	2.265
Section:	
Tip	NACA 0012-69 Modified
Root	NACA 0010-Modified
Vertical tail:	
Span, m (ft)	0.220 (0.721)
Chord:	
Tip, m (ft)	0.081 (0.265)
Root, m (ft)	0.200 (0.656)
Mean, m (ft)	0.149 (0.488)
Area	0.033 (0.355)
Aspect ratio	1.675
Section	10^o symmetrical: 60^o to 40^o wedge

(c) Booster tank

Length, m (ft)	1.388 (4.555)
Diameter, m (ft)	0.241 (0.790)

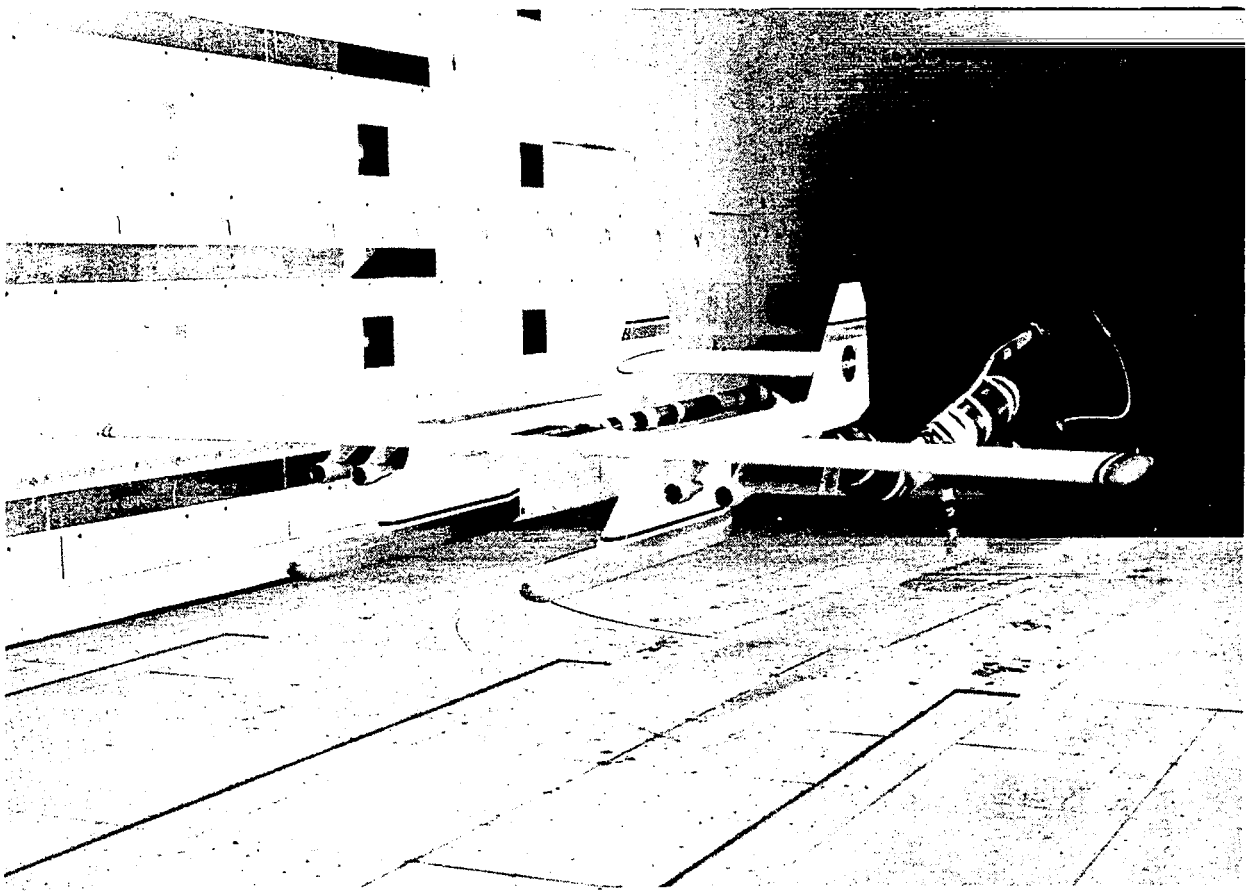

L-74-4545

Figure 1.- Installation of transport model in V/STOL tunnel.

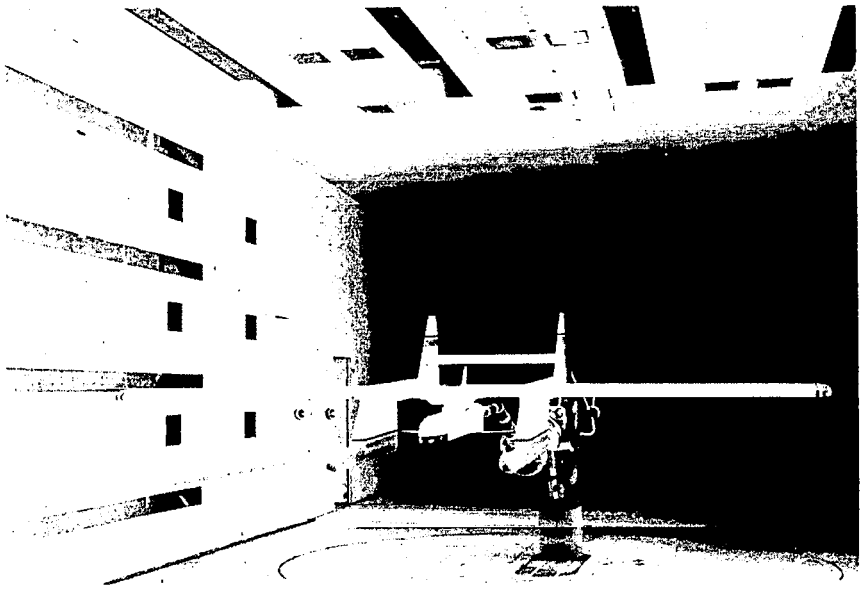

(a) Transport and orbiter. L-74-4544

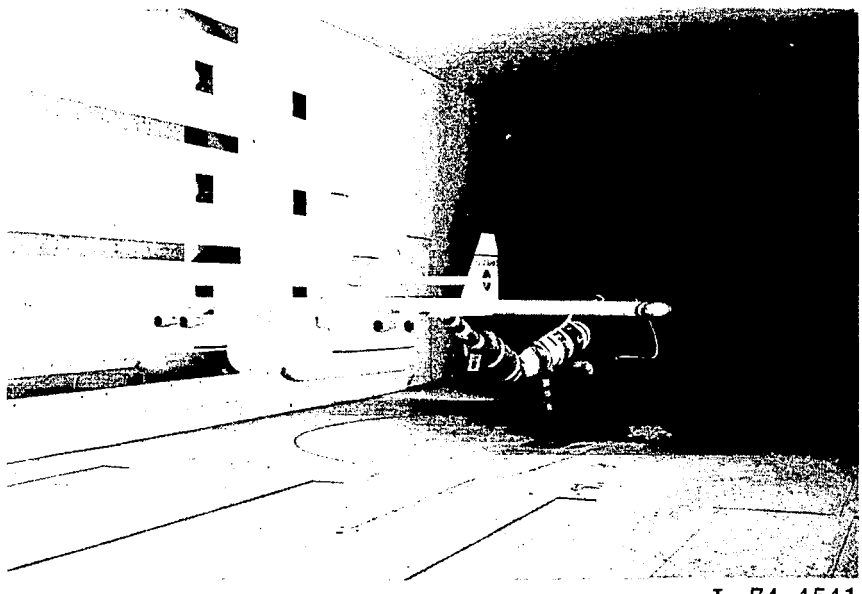

(b) Transport and booster tank. L-74-4541

Figure 2.- Installation of transport model with payloads in V/STOL tunnel.

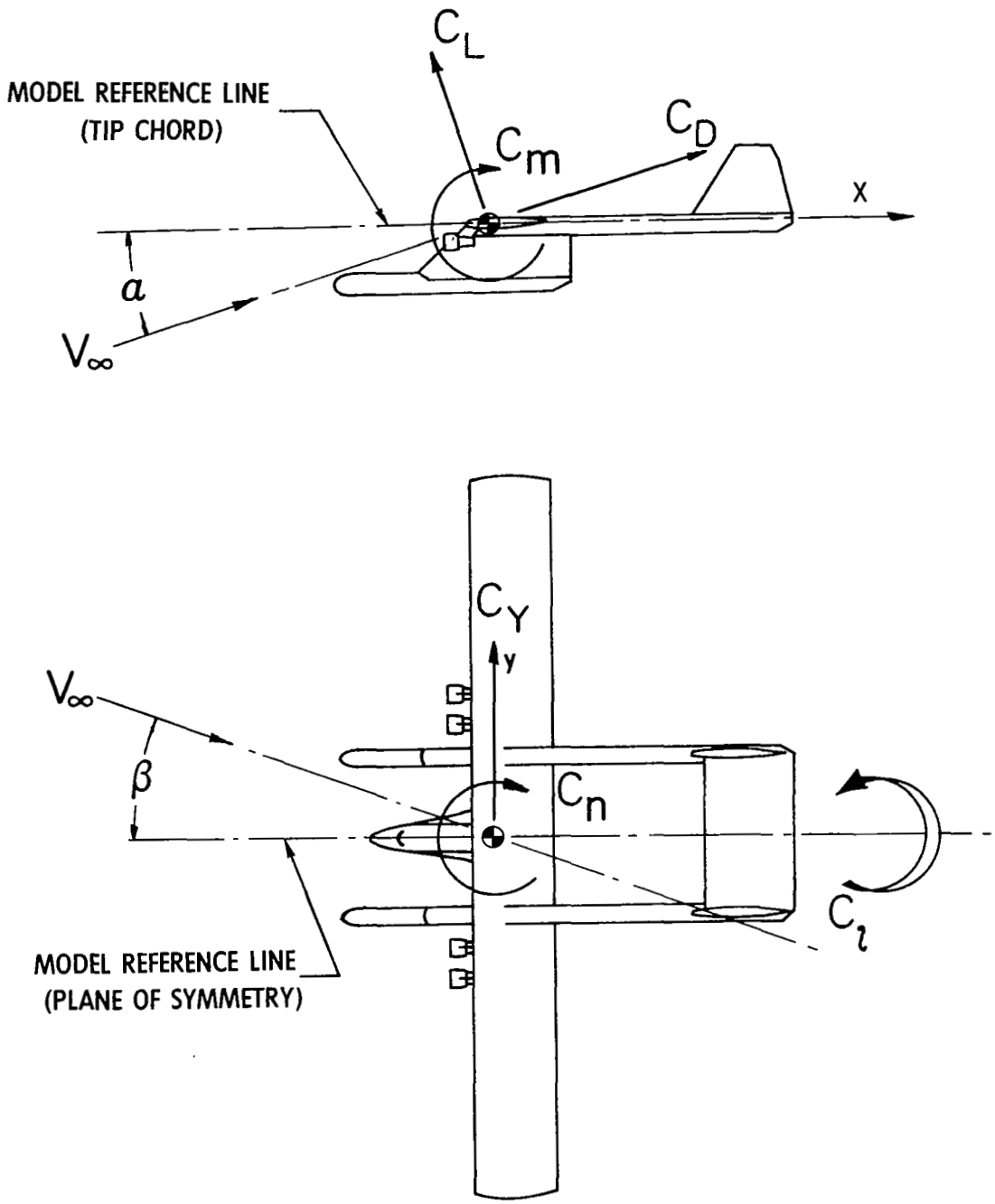

Figure 3.- Stability-axis system used for data presentation.

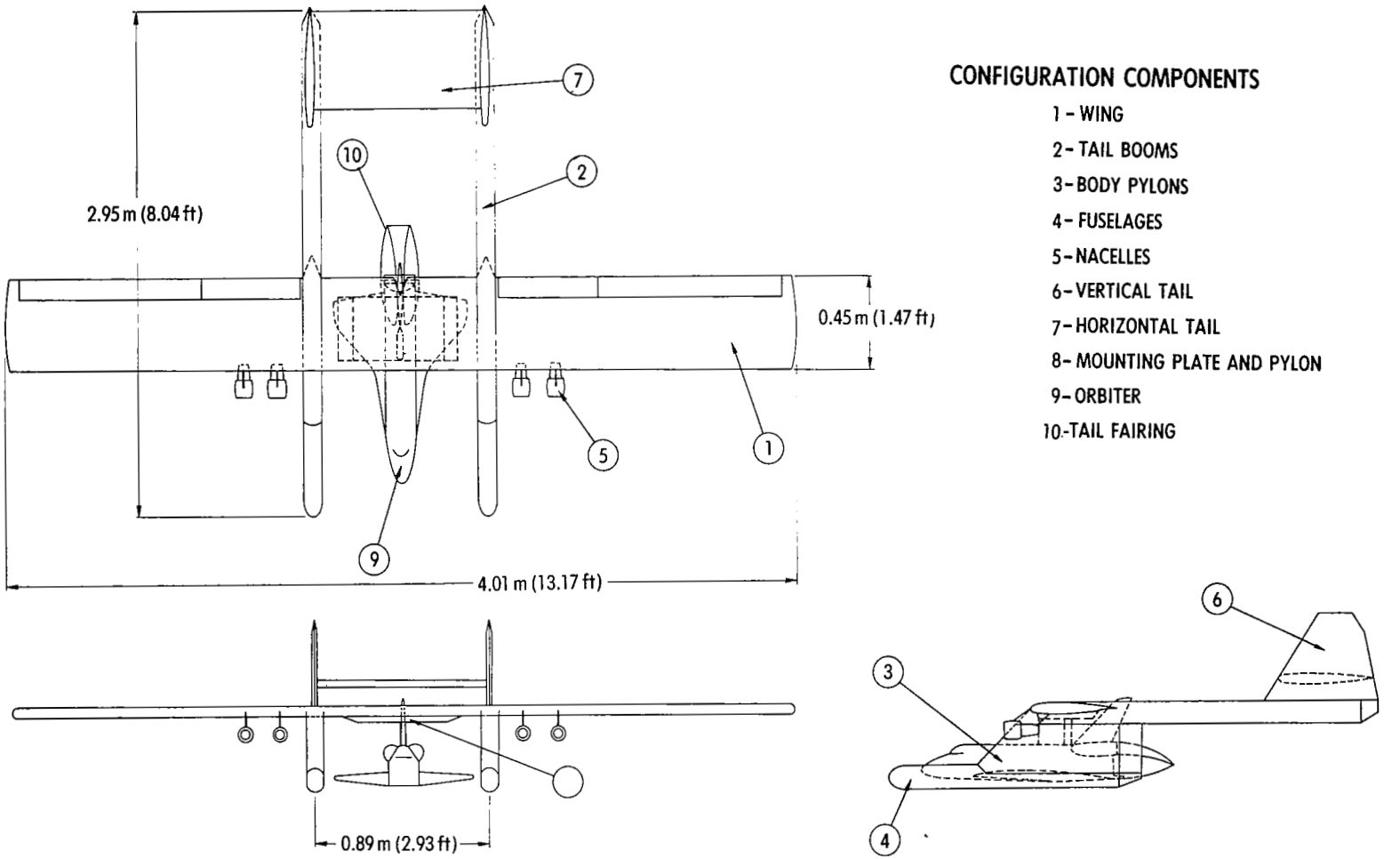

Figure 4.- Three-view drawing of transport model with orbiter payload.

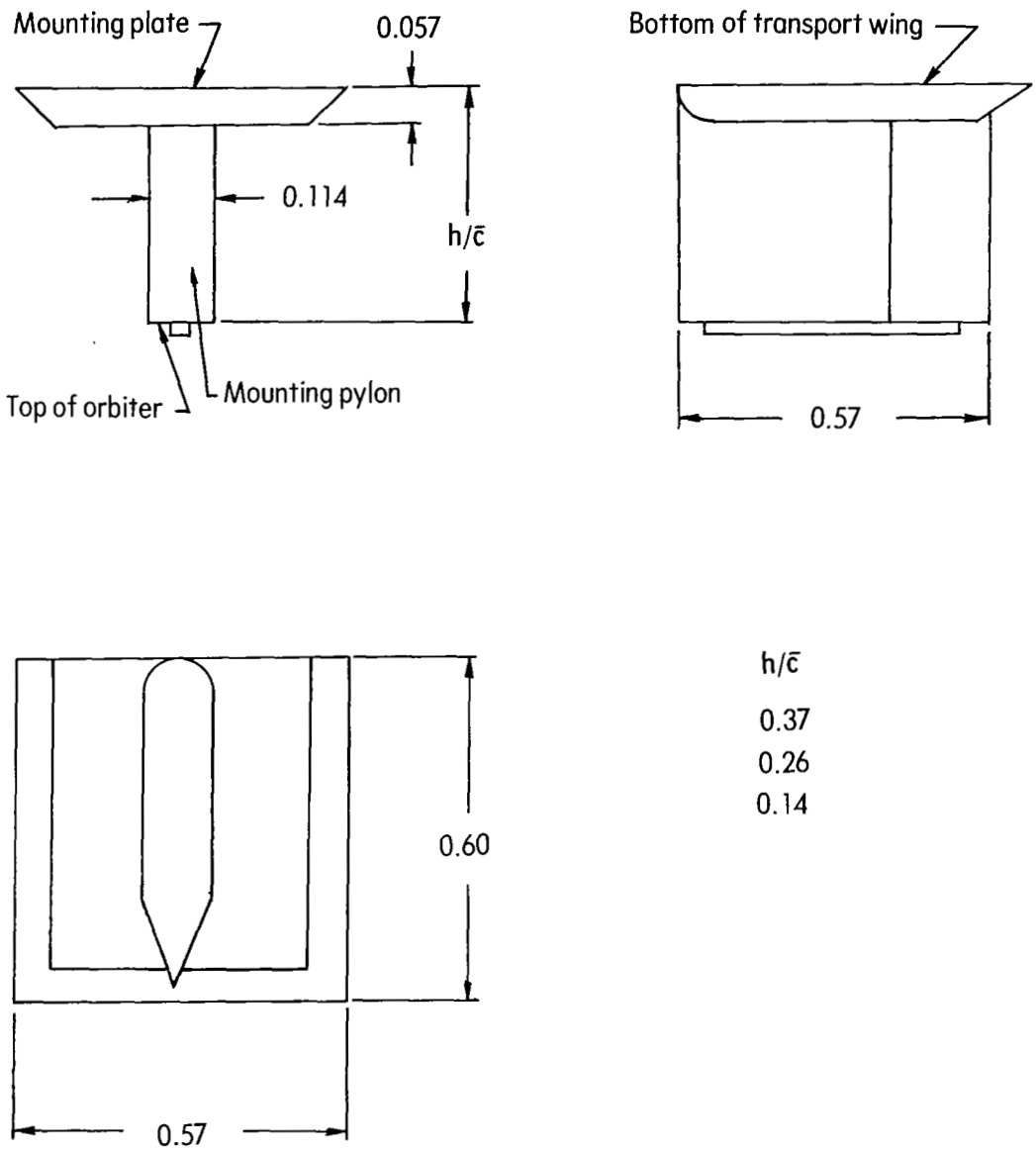

Figure 5.- Three-view drawing of mounting plate and mounting pylon.

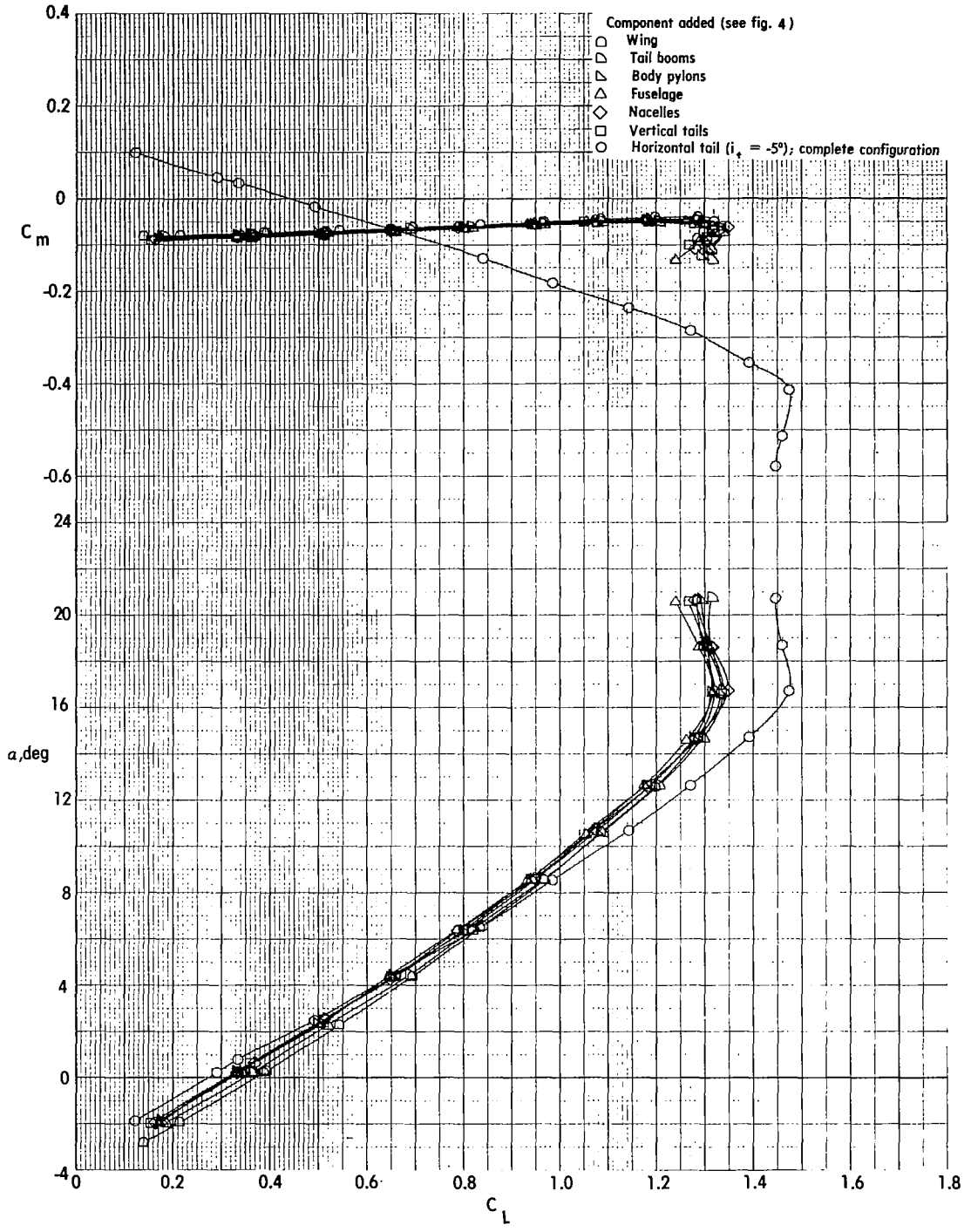

(a) Variation of C_m and α with C_L.

Figure 6.- Longitudinal characteristics of transport model component buildup.

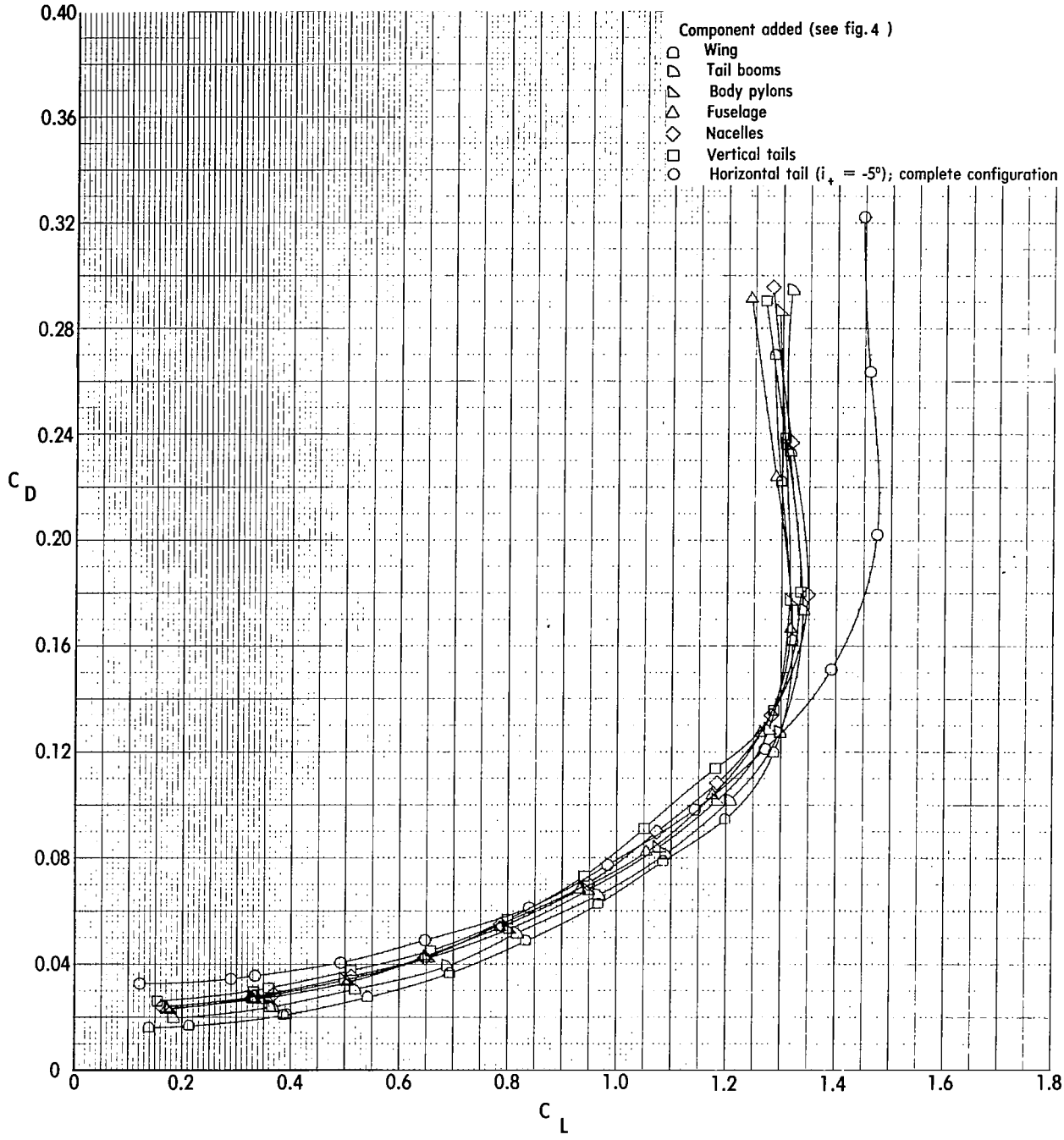

(b) Variation of C_D with C_L.

Figure 6.- Concluded.

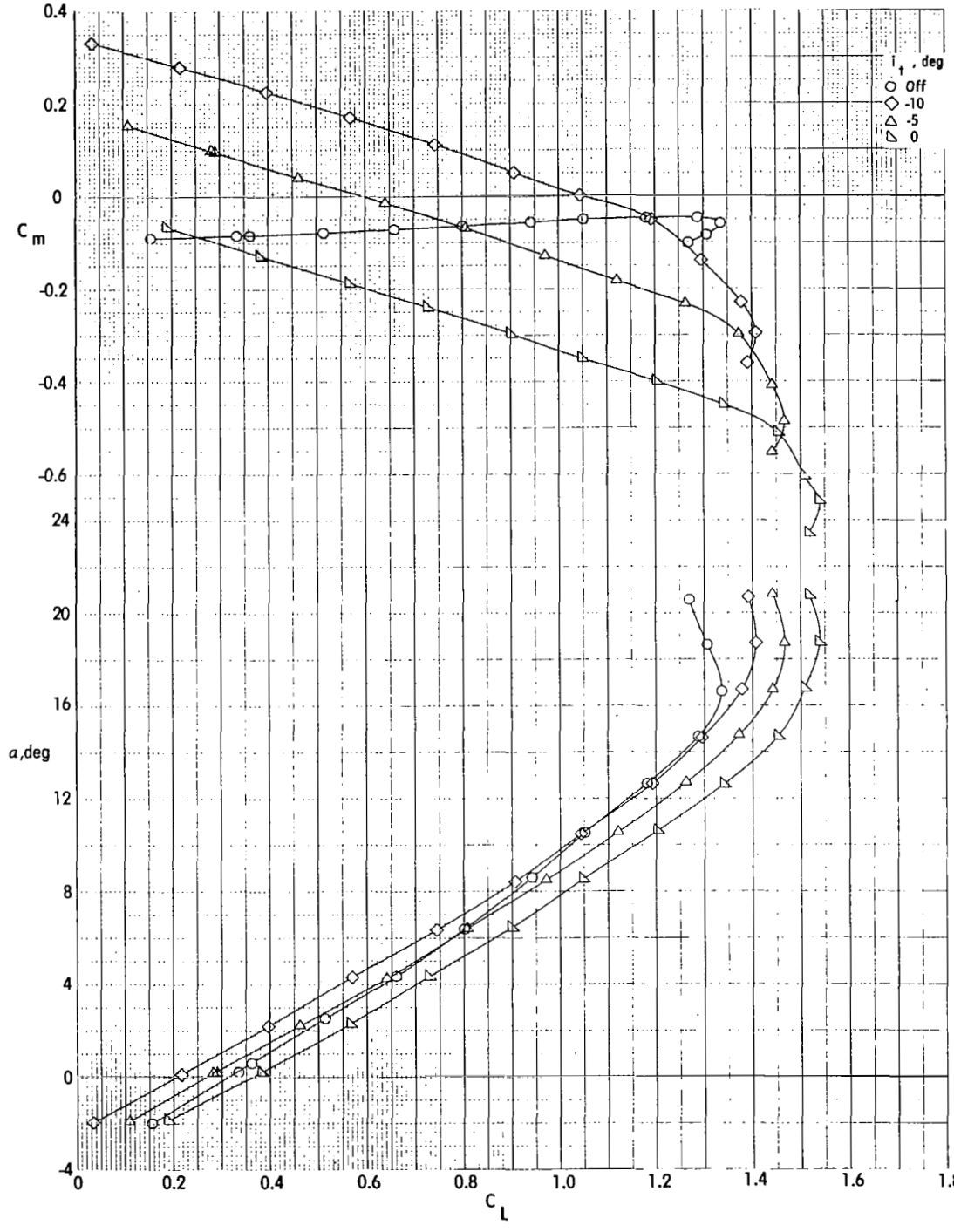

(a) Variation of C_m and α with C_L.

Figure 7.- Longitudinal control characteristics of transport model alone.

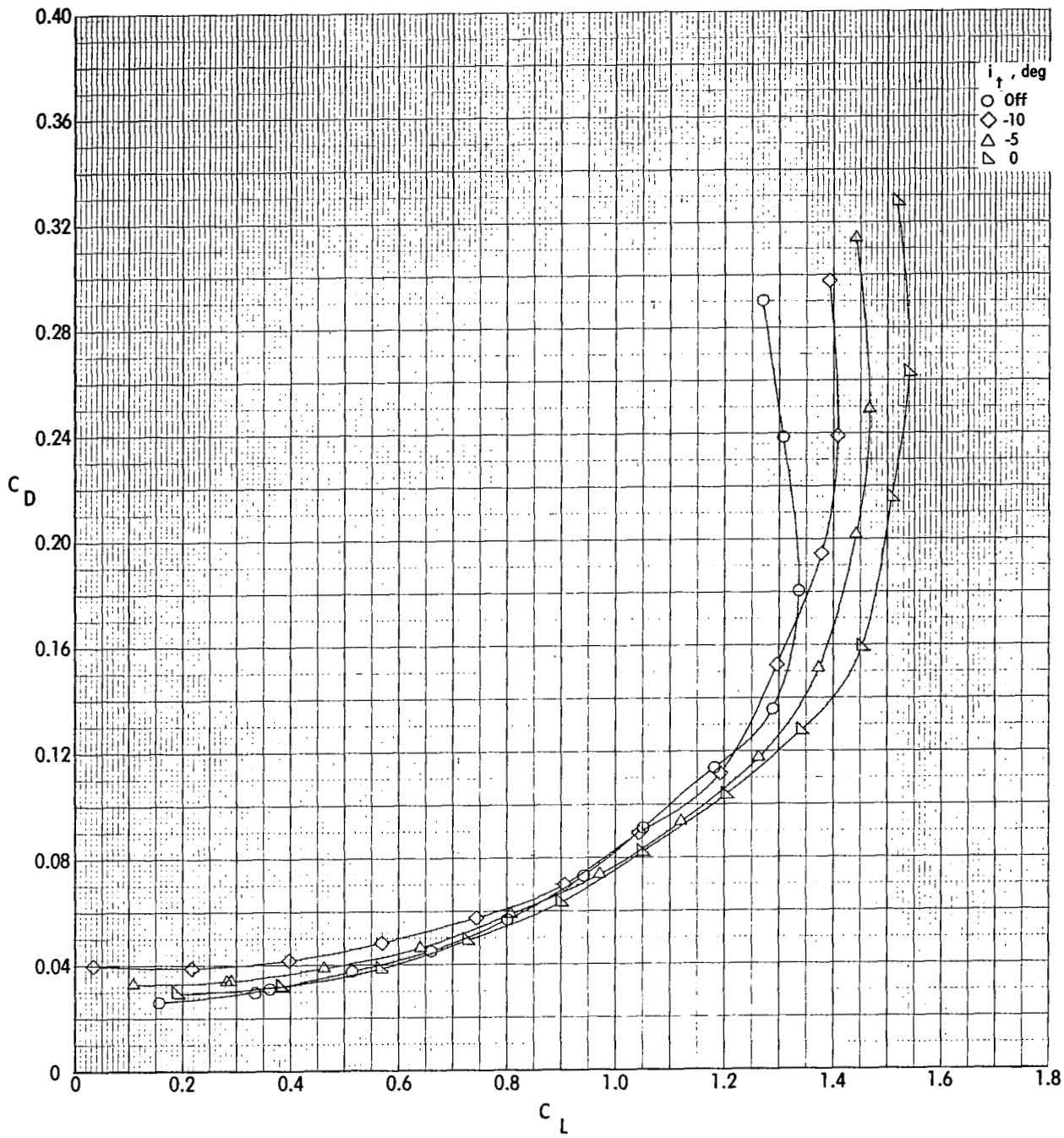

(b) Variation of C_D with C_L.

Figure 7.- Concluded.

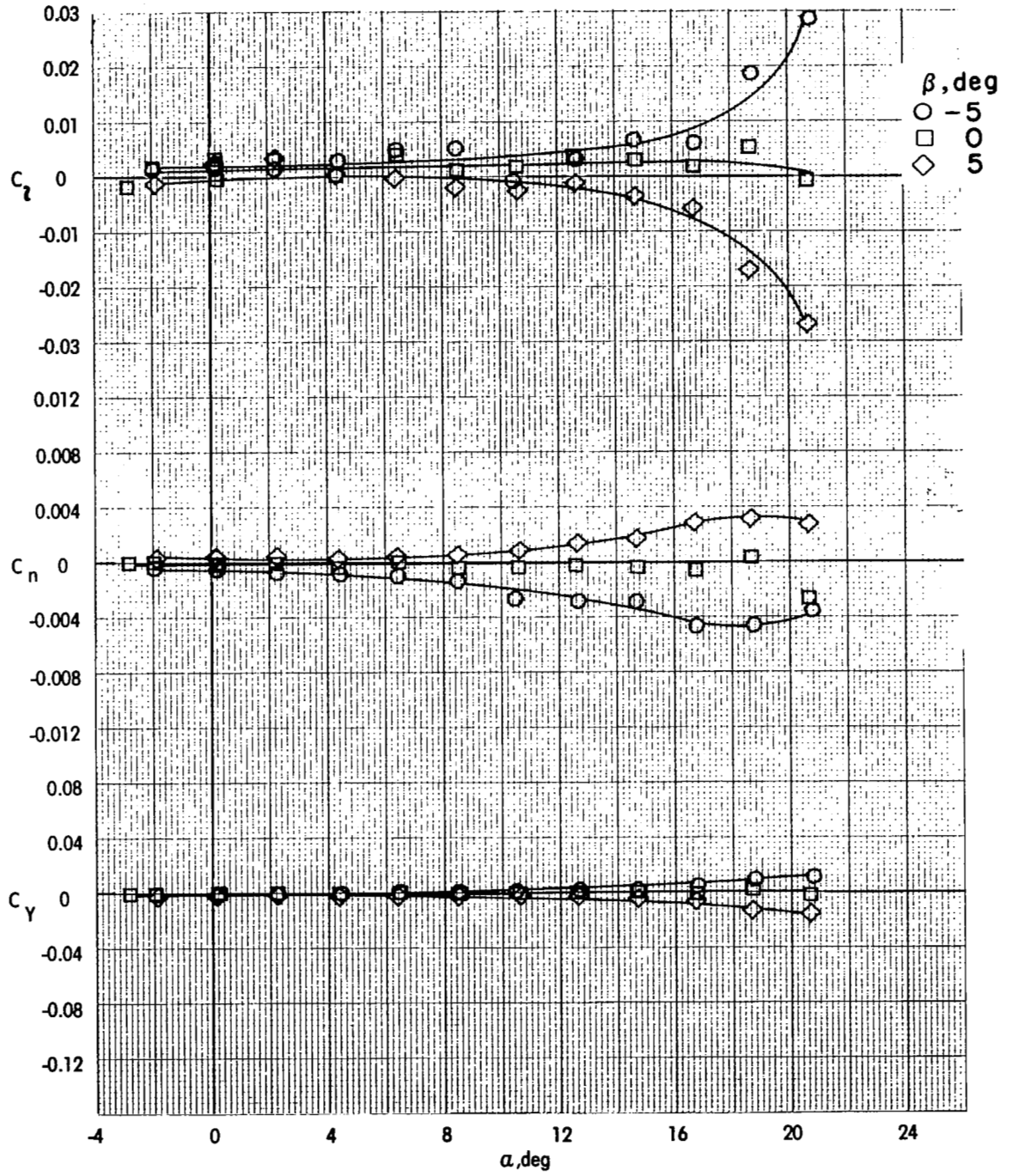

(a) Variation of C_l, C_n, and C_Y with α. (Wing alone.)

Figure 8.- Lateral-directional characteristics of transport model component buildup.

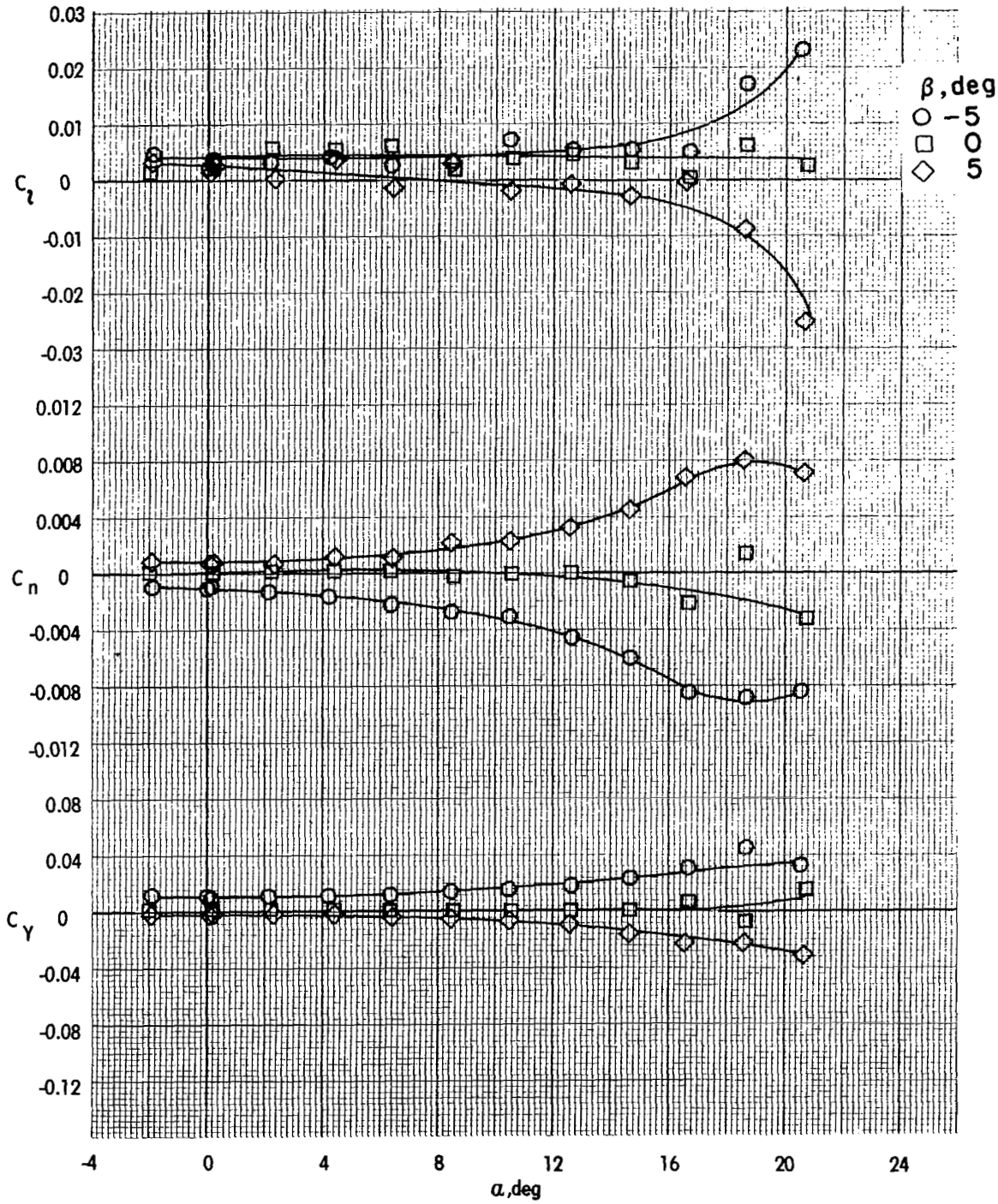

(b) Variation of C_l, C_n, and C_Y with α. (Addition of tail booms.)

Figure 8.- Continued.

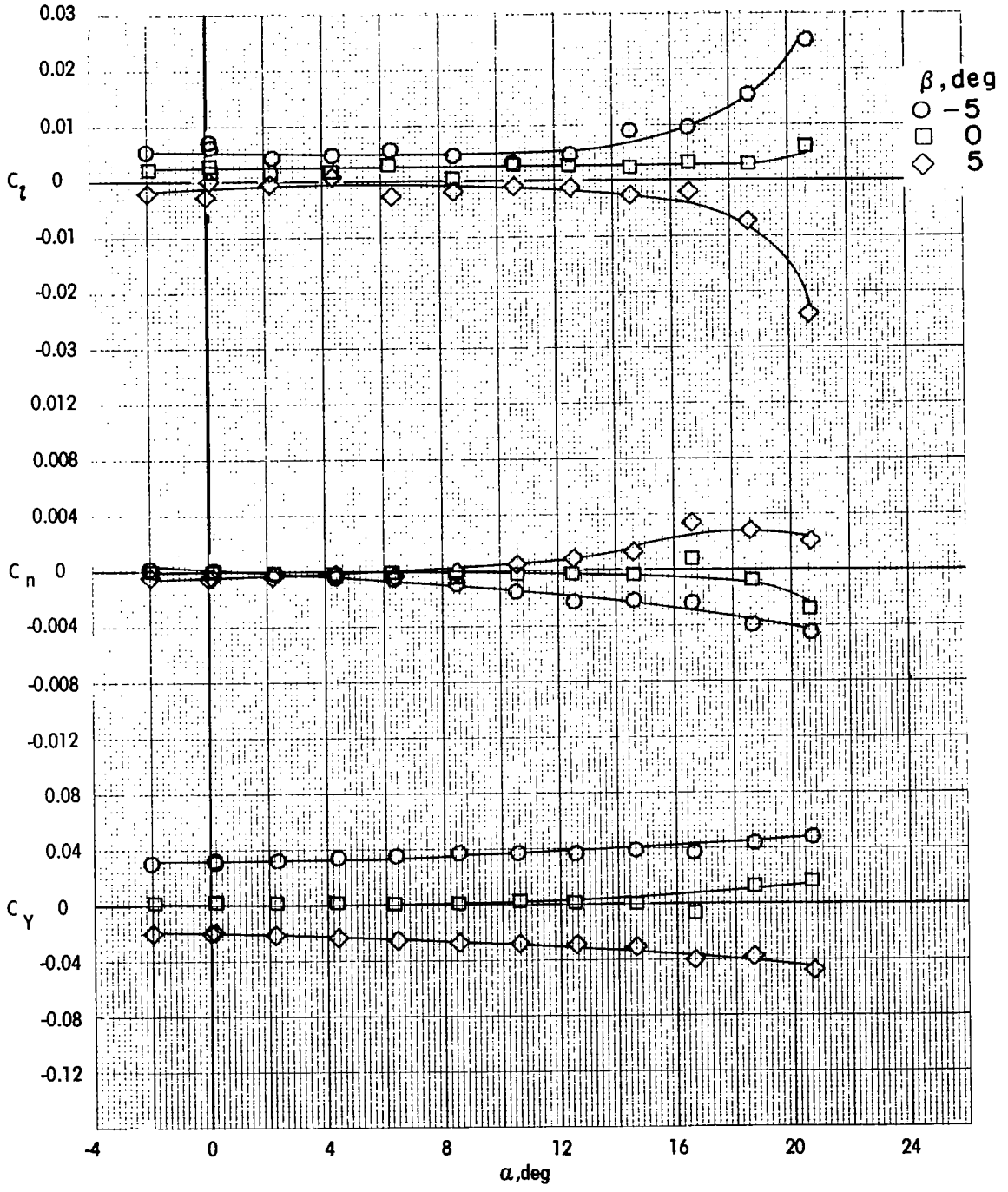

(c) Variation of C_l, C_n, and C_Y with α. (Addition of body pylons.)

Figure 8.- Continued.

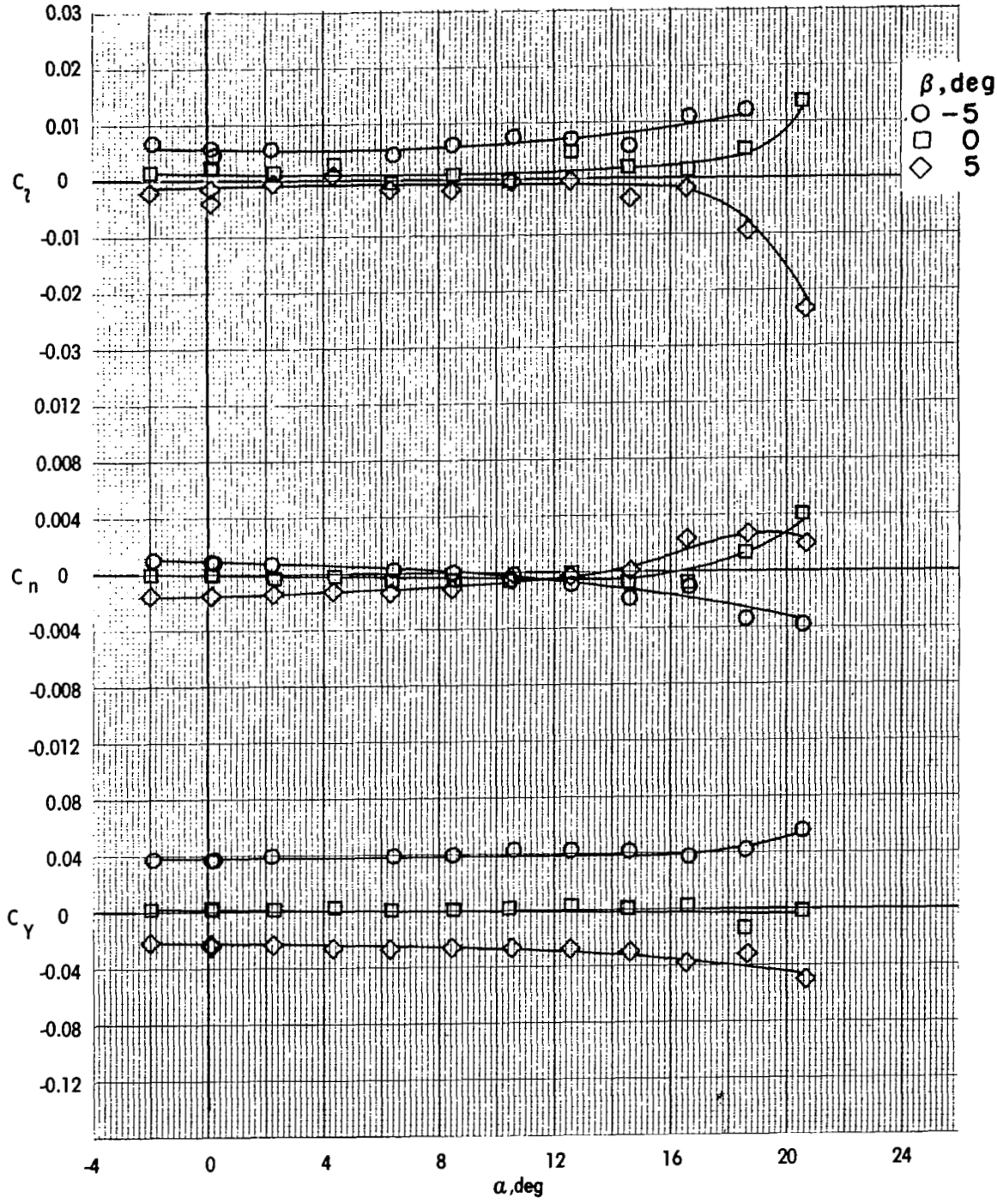

(d) Variation of C_l, C_n, and C_Y with α. (Addition of fuselages.)

Figure 8.- Continued.

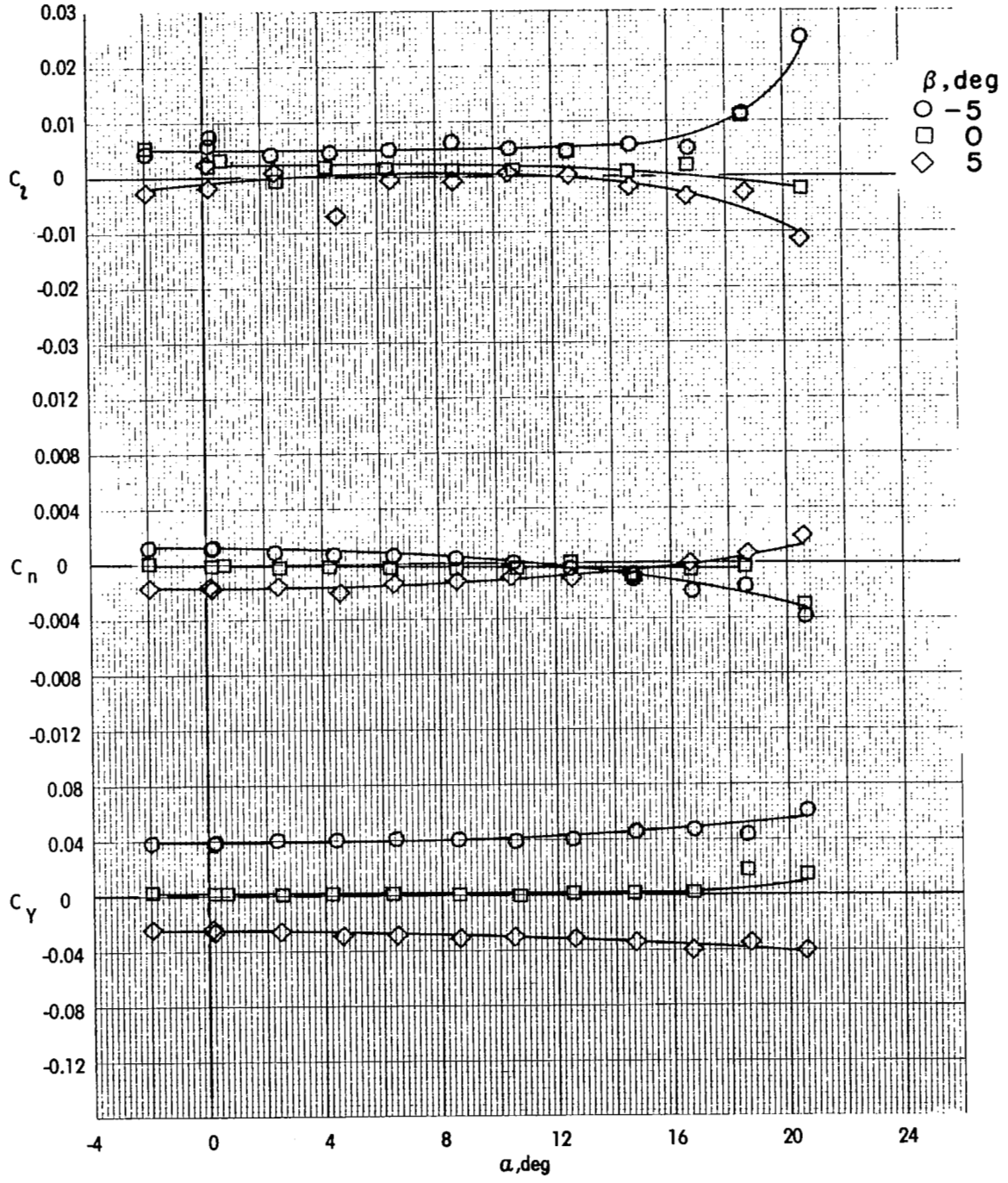

(e) Variation of C_l, C_n, and C_Y with α. (Addition of nacelles.)

Figure 8.- Continued.

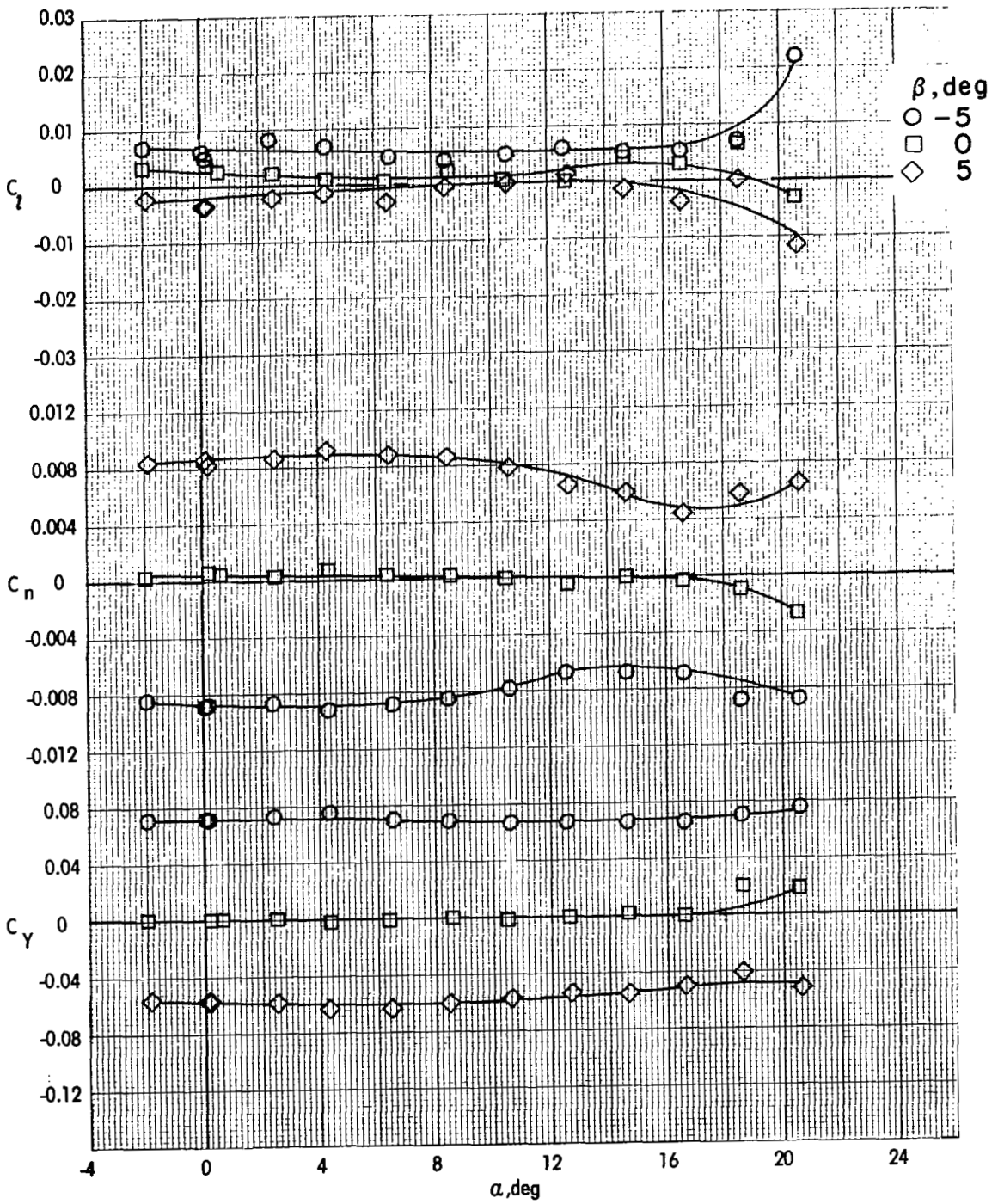

(f) Variation of C_l, C_n, and C_Y with α. (Addition of vertical tails.)

Figure 8.- Continued.

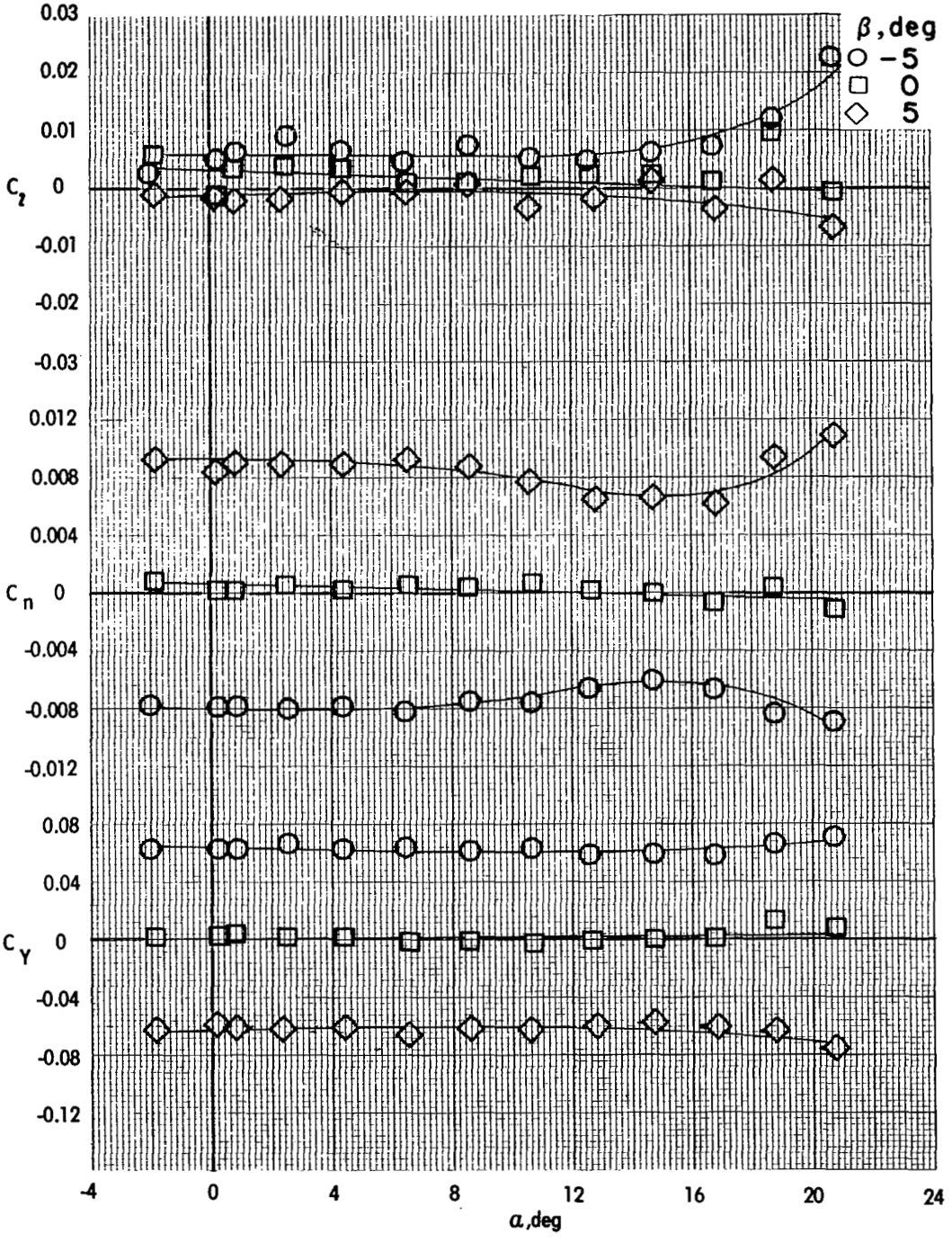

(g) Variation of C_l, C_n, and C_Y with α. (Complete transport, $i_t = -5^o$.)

Figure 8.- Concluded.

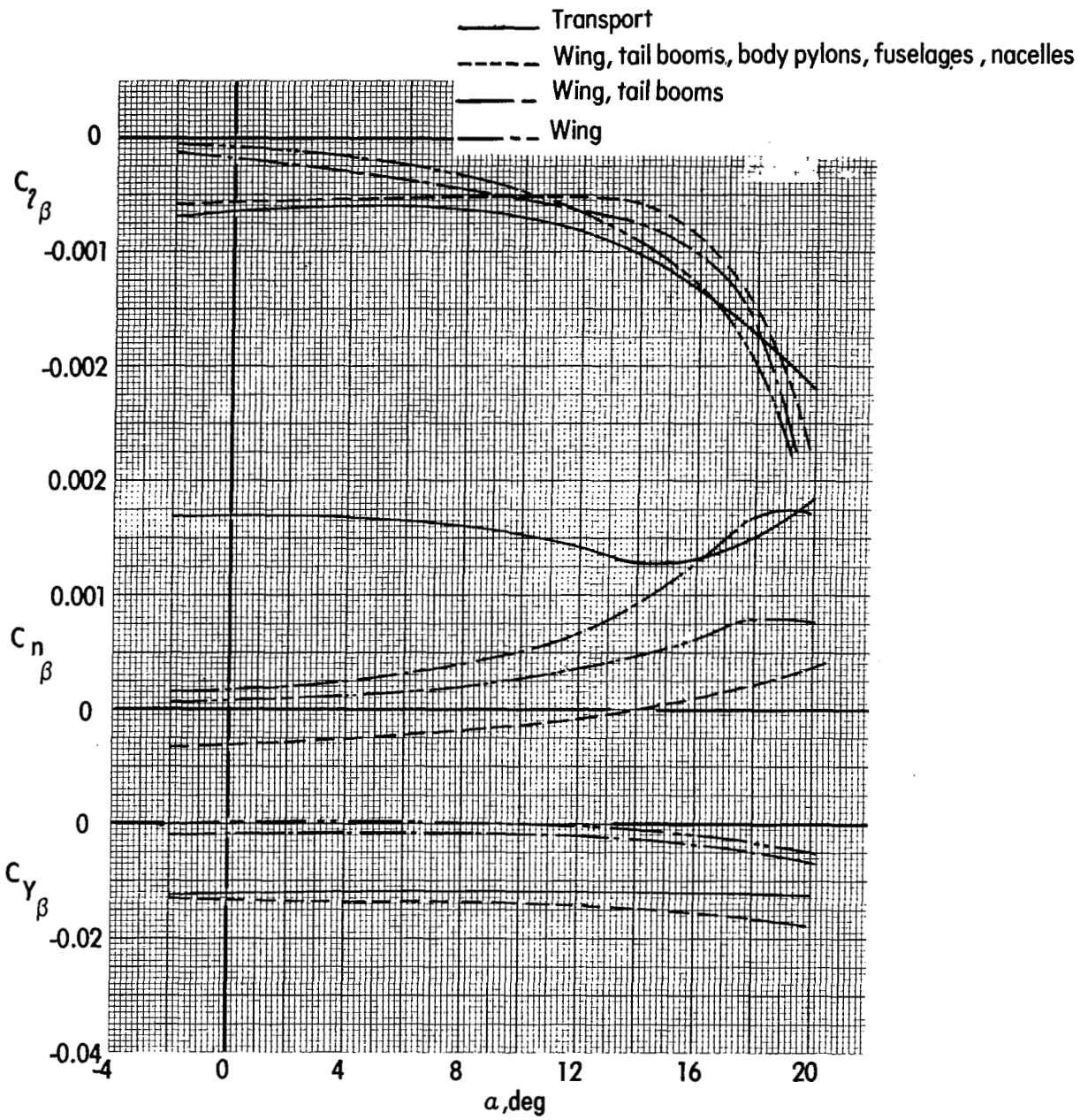

Figure 9.- Lateral-directional stability derivatives for transport model component buildup.

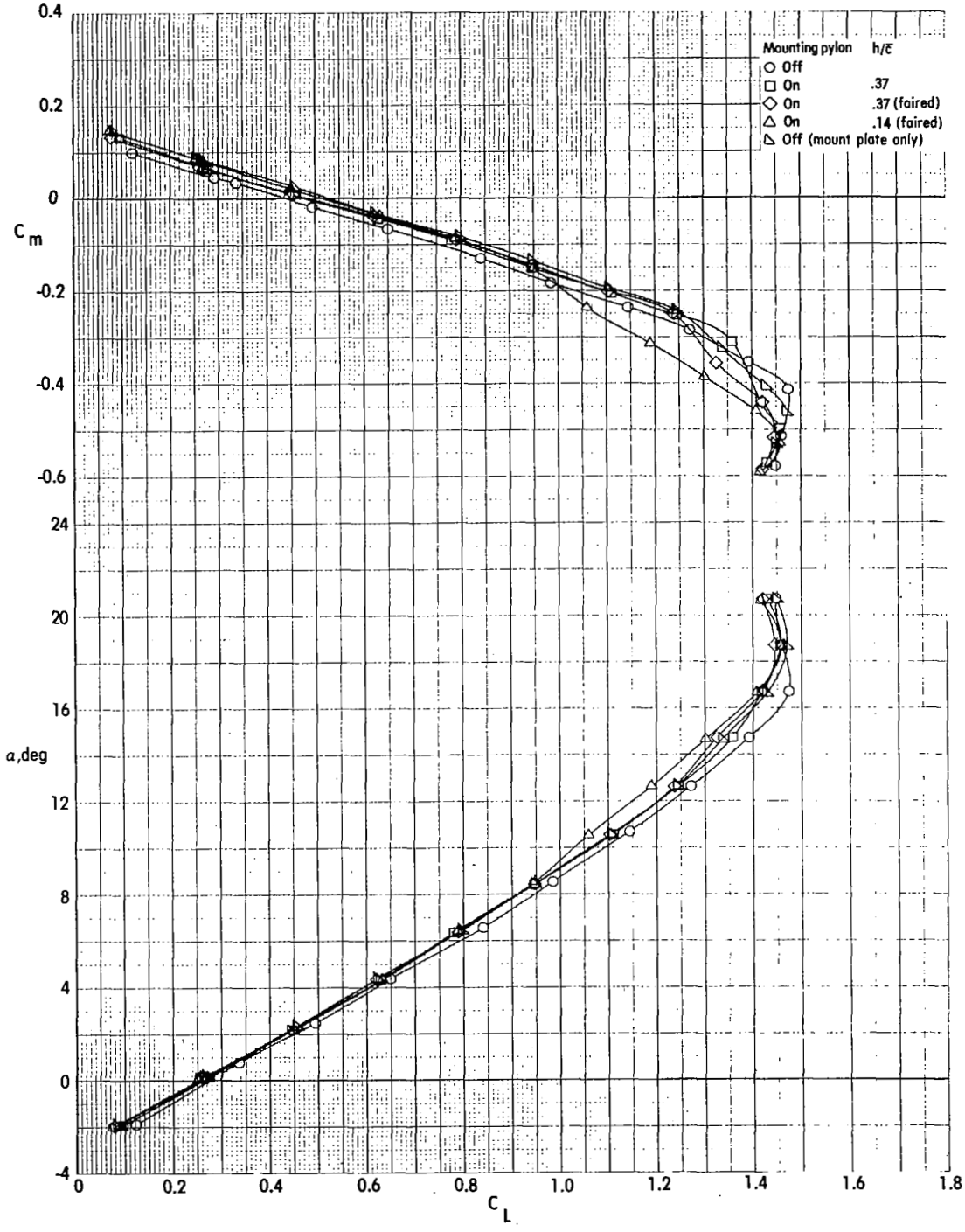

(a) Variation of C_m and α with C_L.

Figure 10.- Longitudinal characteristics of transport model $(i_t = -5^o)$ with mounting plate and mounting pylon.

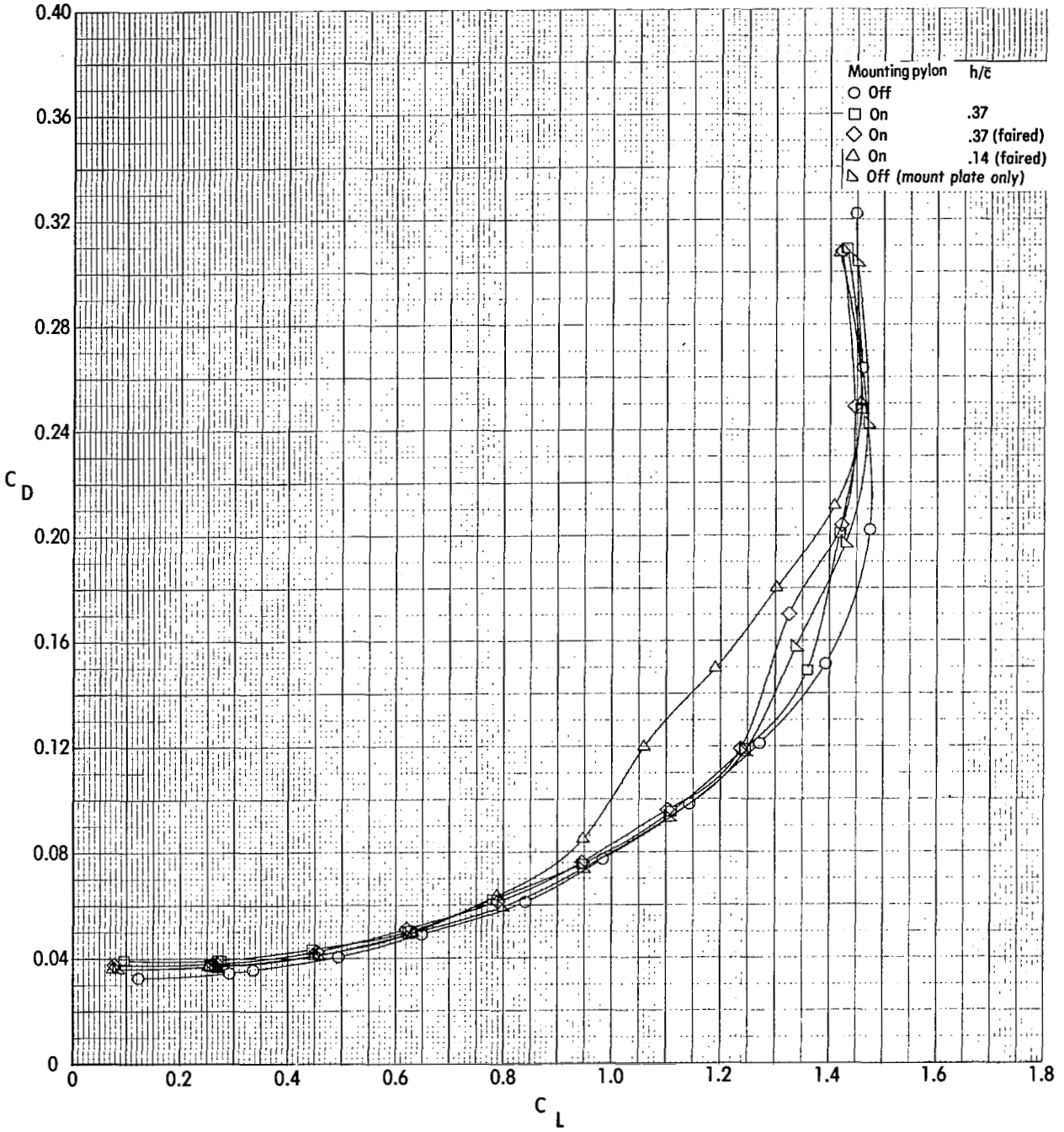

(b) Variation of C_D with C_L.

Figure 10.- Concluded.

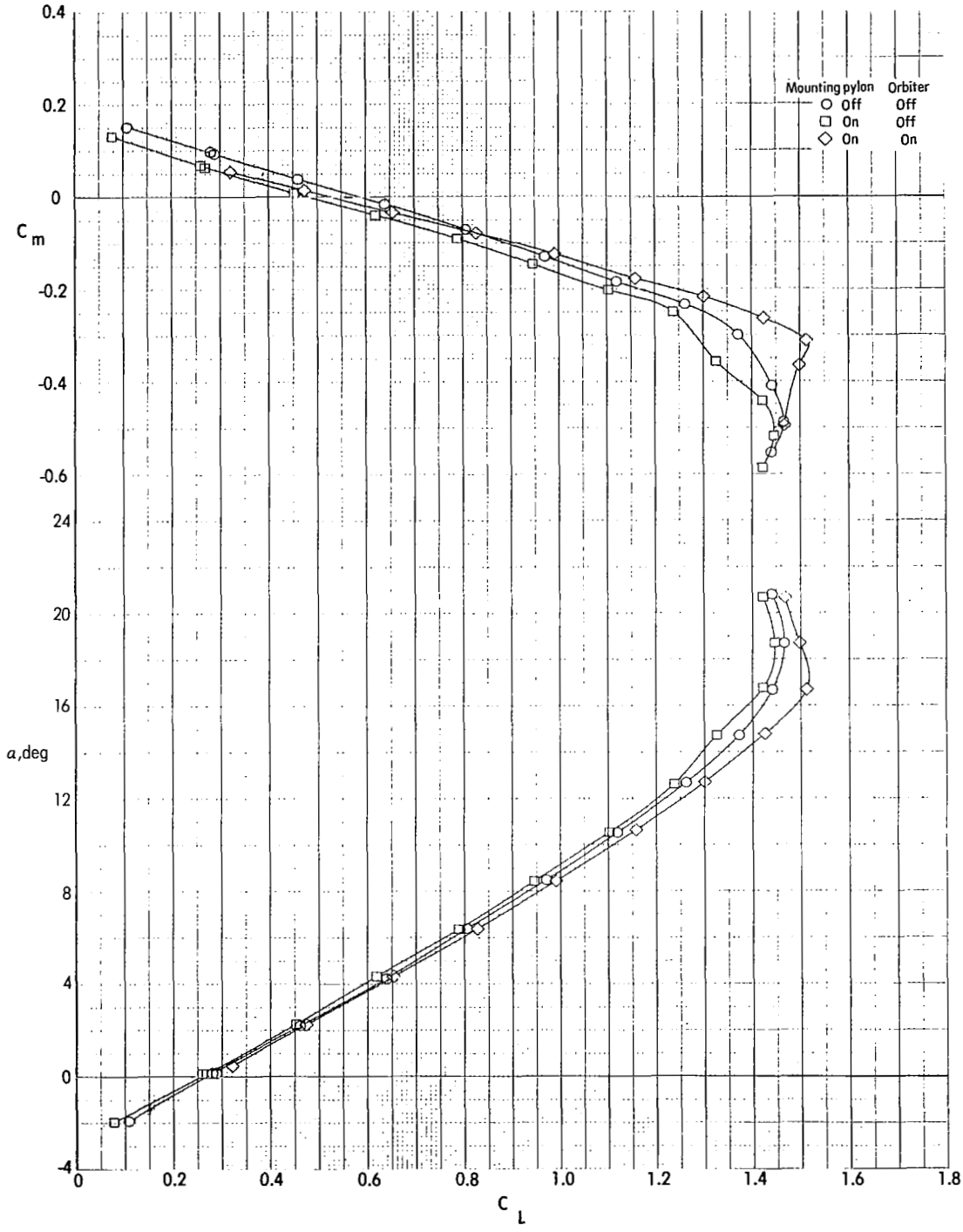

(a) Variation of C_m and α with C_L. ($h/\bar{c} = 0.37$.)

Figure 11.- Longitudinal characteristics of transport model ($i_t = -5^o$) with orbiter payload.

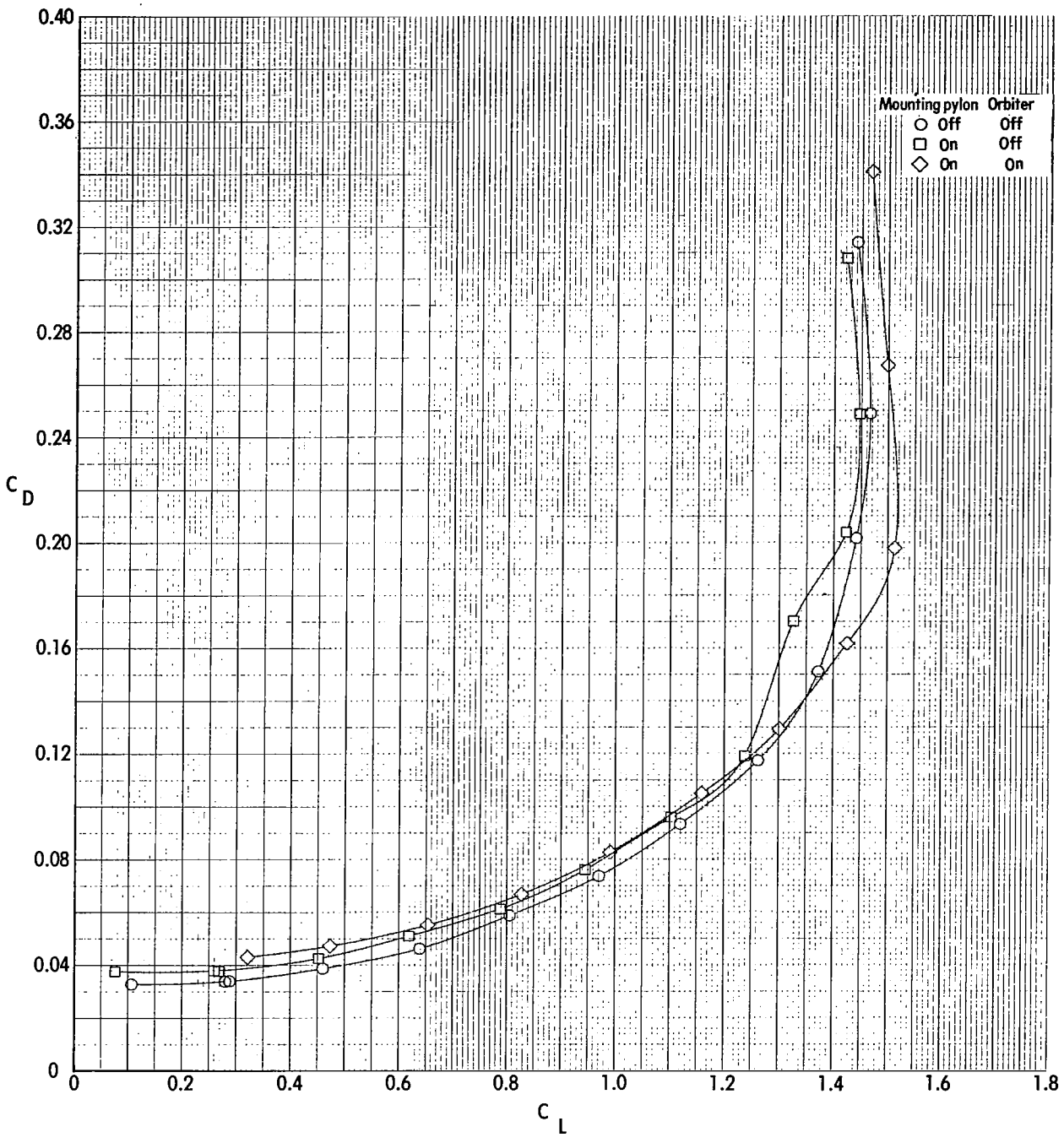

(b) Variation of C_D with C_L. ($h/\bar{c} = 0.37$.)

Figure 11.- Continued.

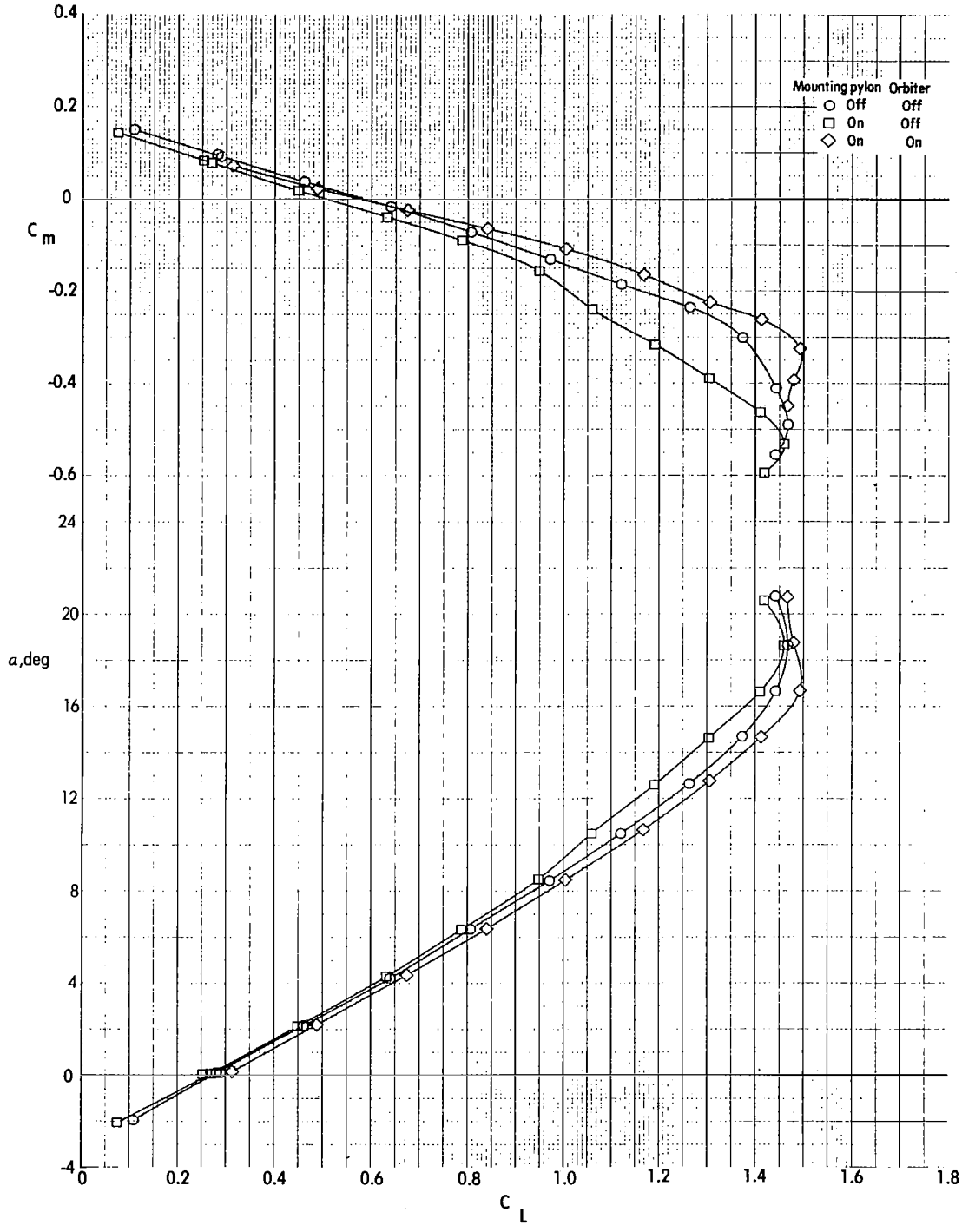

(c) Variation of C_m and α with C_L. ($h/\bar{c} = 0.14$.)

Figure 11.- Continued.

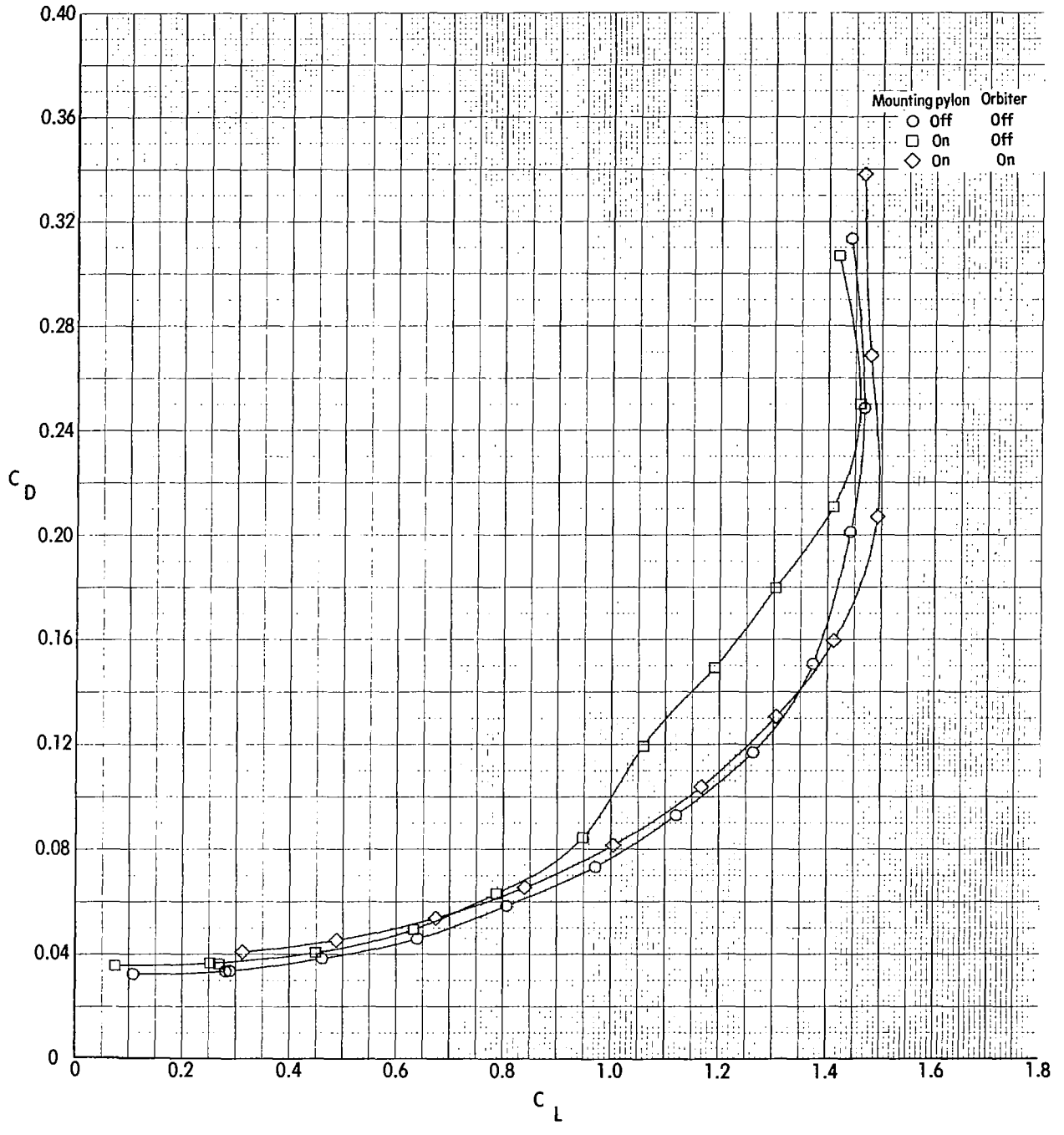

(d) Variation of C_D with C_L. ($h/\bar{c} = 0.14$.)

Figure 11.- Concluded.

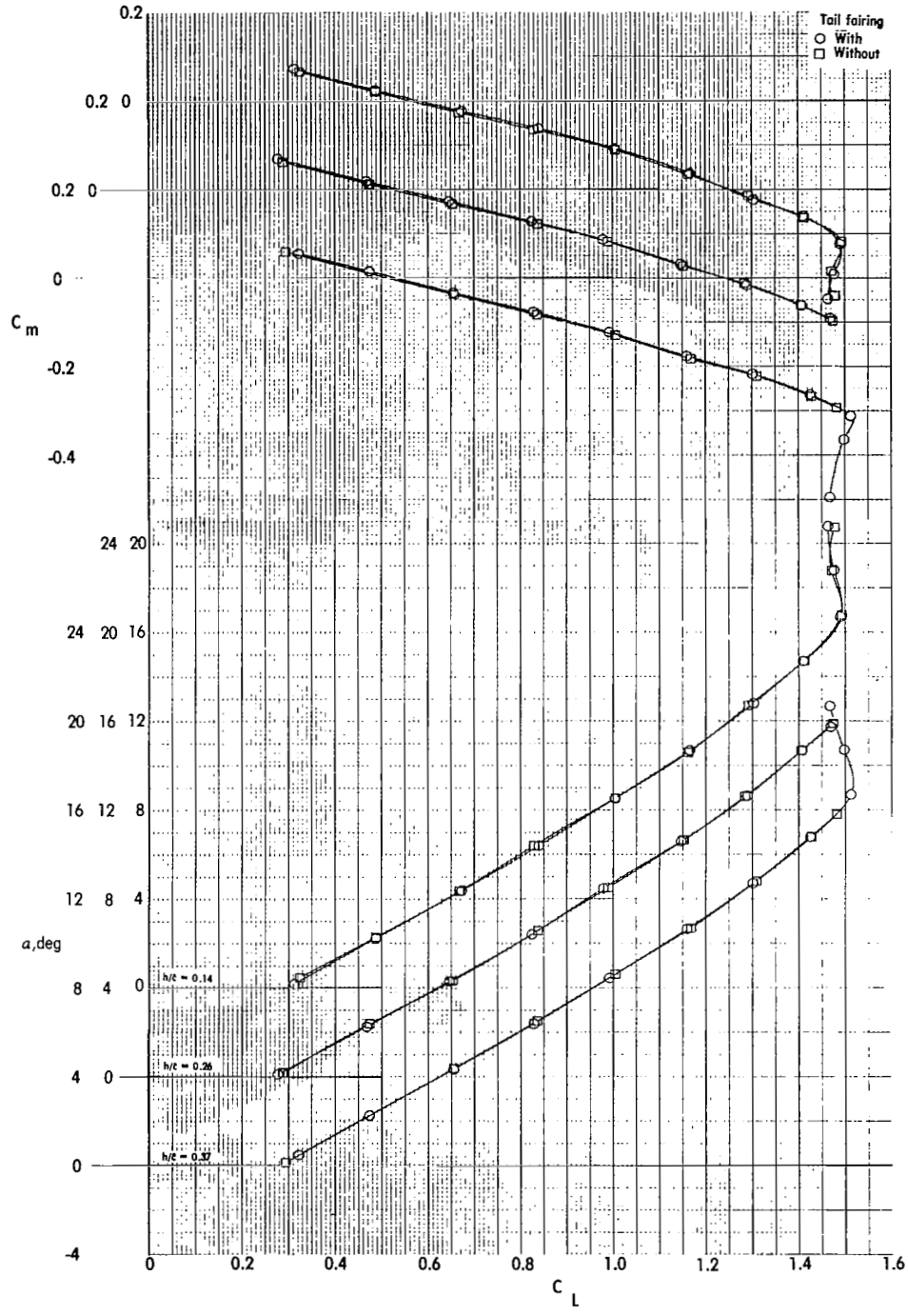

(a) Variation of C_m and α with C_L.

Figure 12.- Longitudinal characteristics of transport model $(i_t = -5^o)$ with orbiter payload $(x/\bar{c} = 0.25)$ with and without orbiter tail fairing.

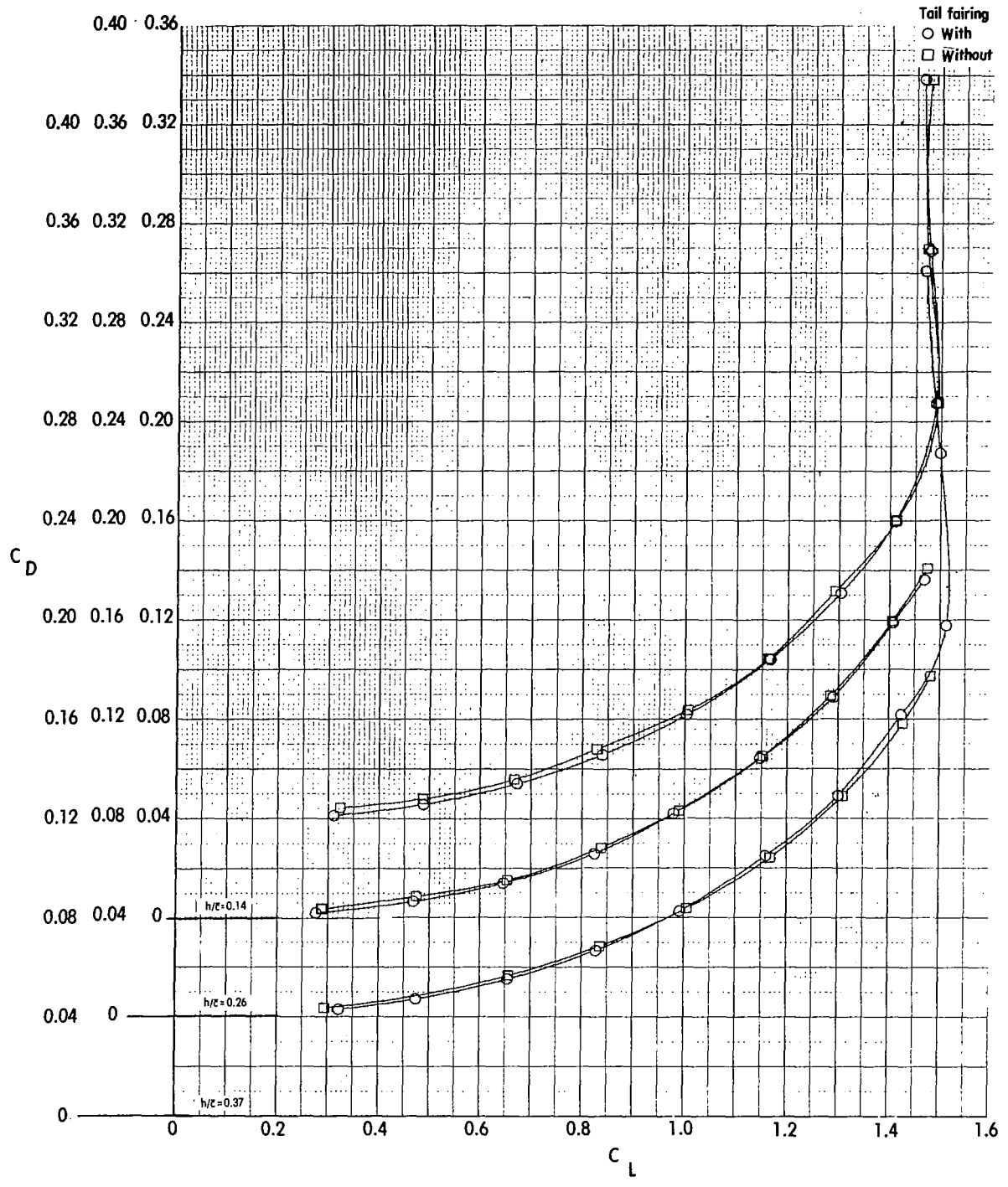

(b) Variation of C_D with C_L.

Figure 12.- Concluded.

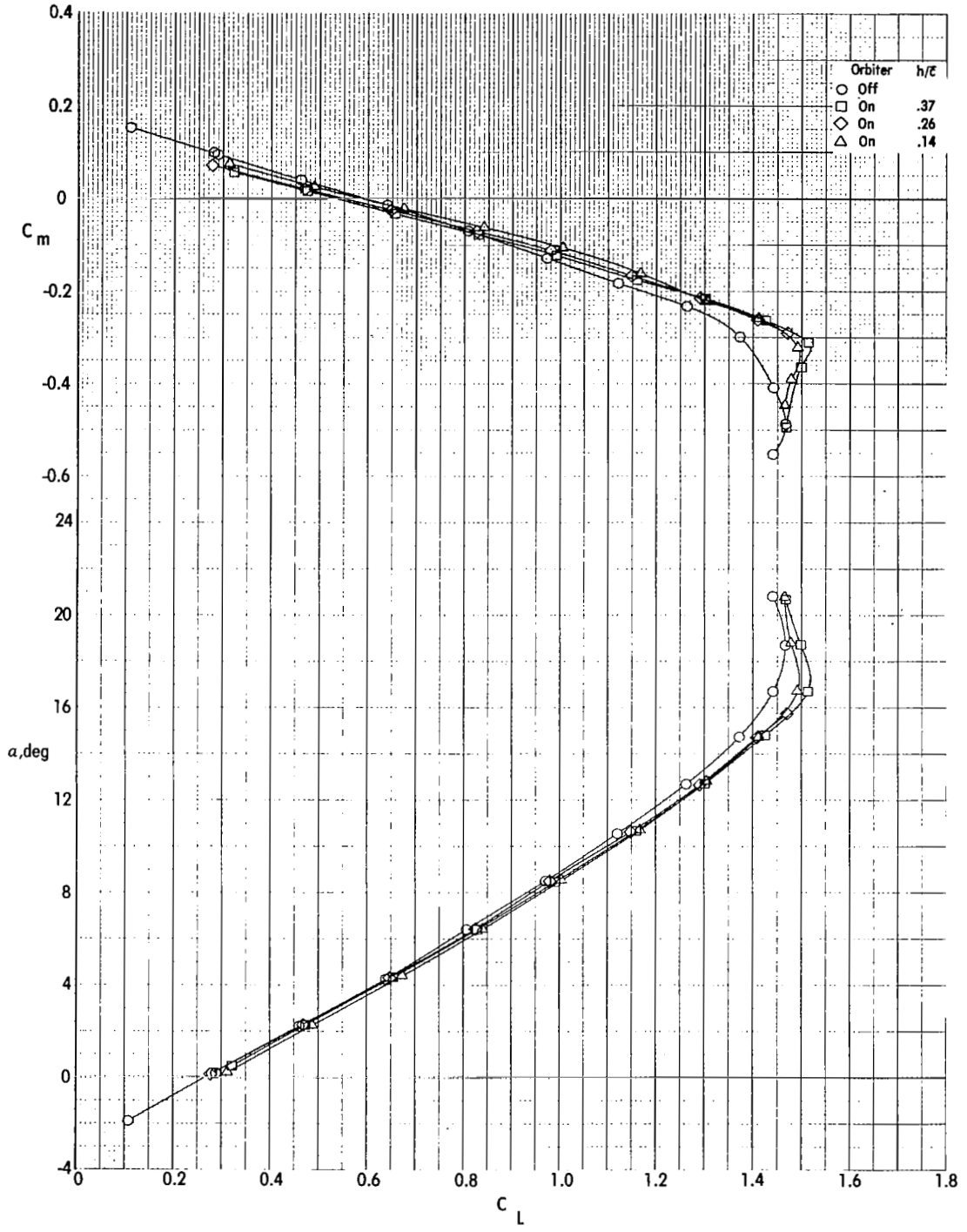

(a) Variation of C_m and α with C_L.

Figure 13.- Longitudinal characteristics of transport model $(i_t = -5^o)$ with orbiter payload with tail fairing $(x/\bar{c} = 0.25)$ at various separation distances.

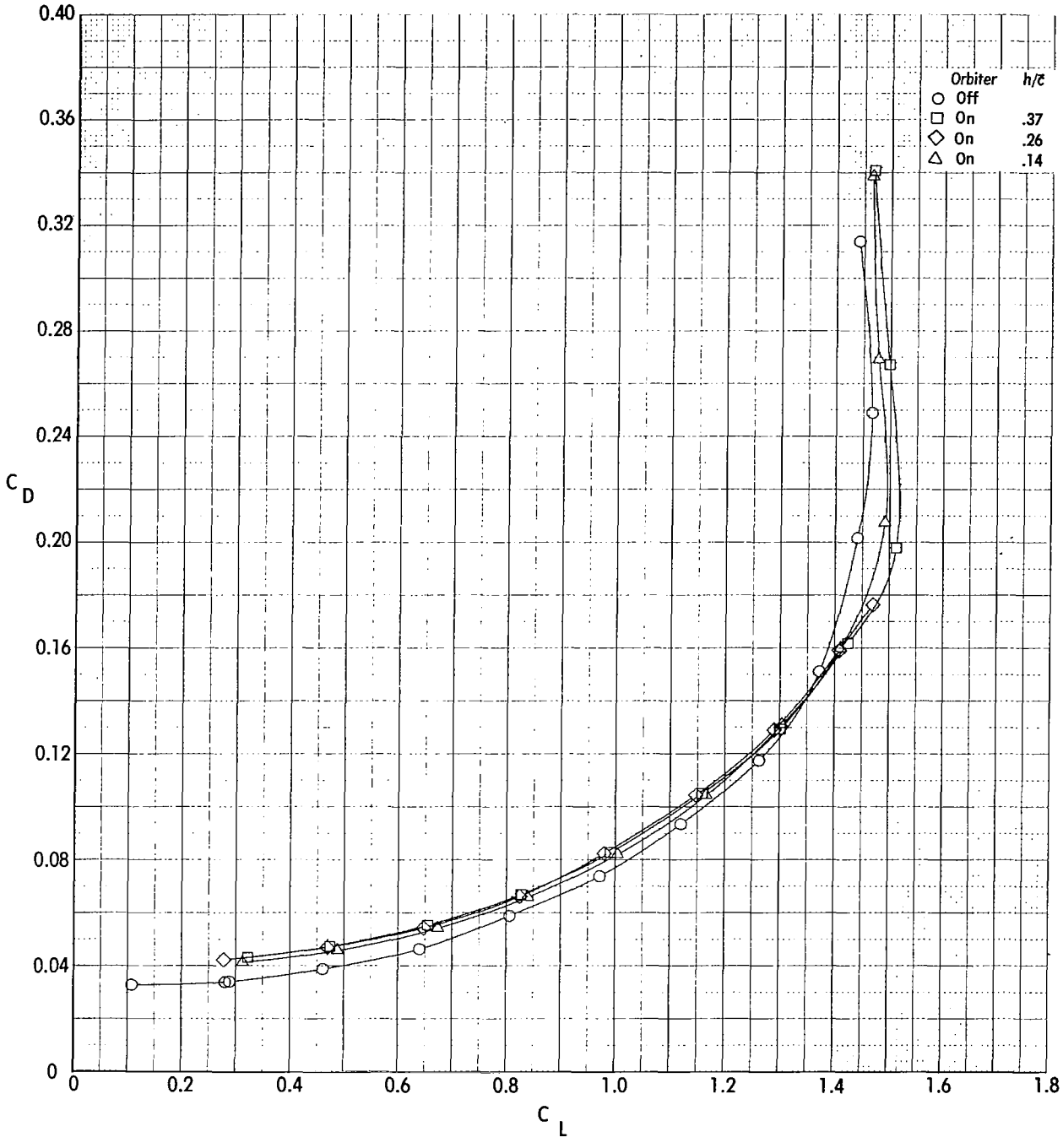

(b) Variation of C_D with C_L.

Figure 13.- Concluded.

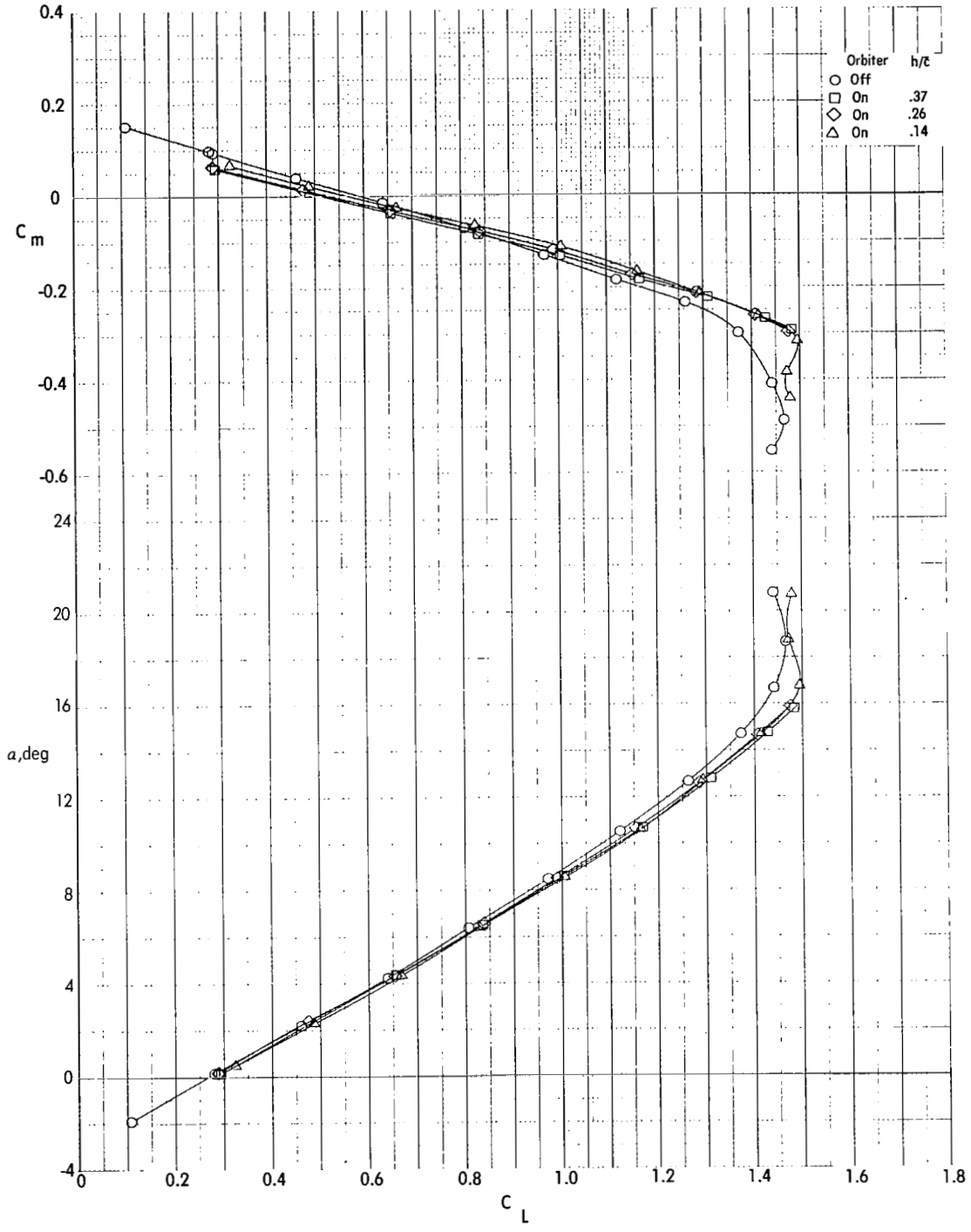

(a) Variation of C_m and α with C_L.

Figure 14.- Longitudinal characteristics of transport model $(i_t = -5^o)$ with orbiter payload without tail fairing $(x/\bar{c} = 0.25)$ at various separation distances.

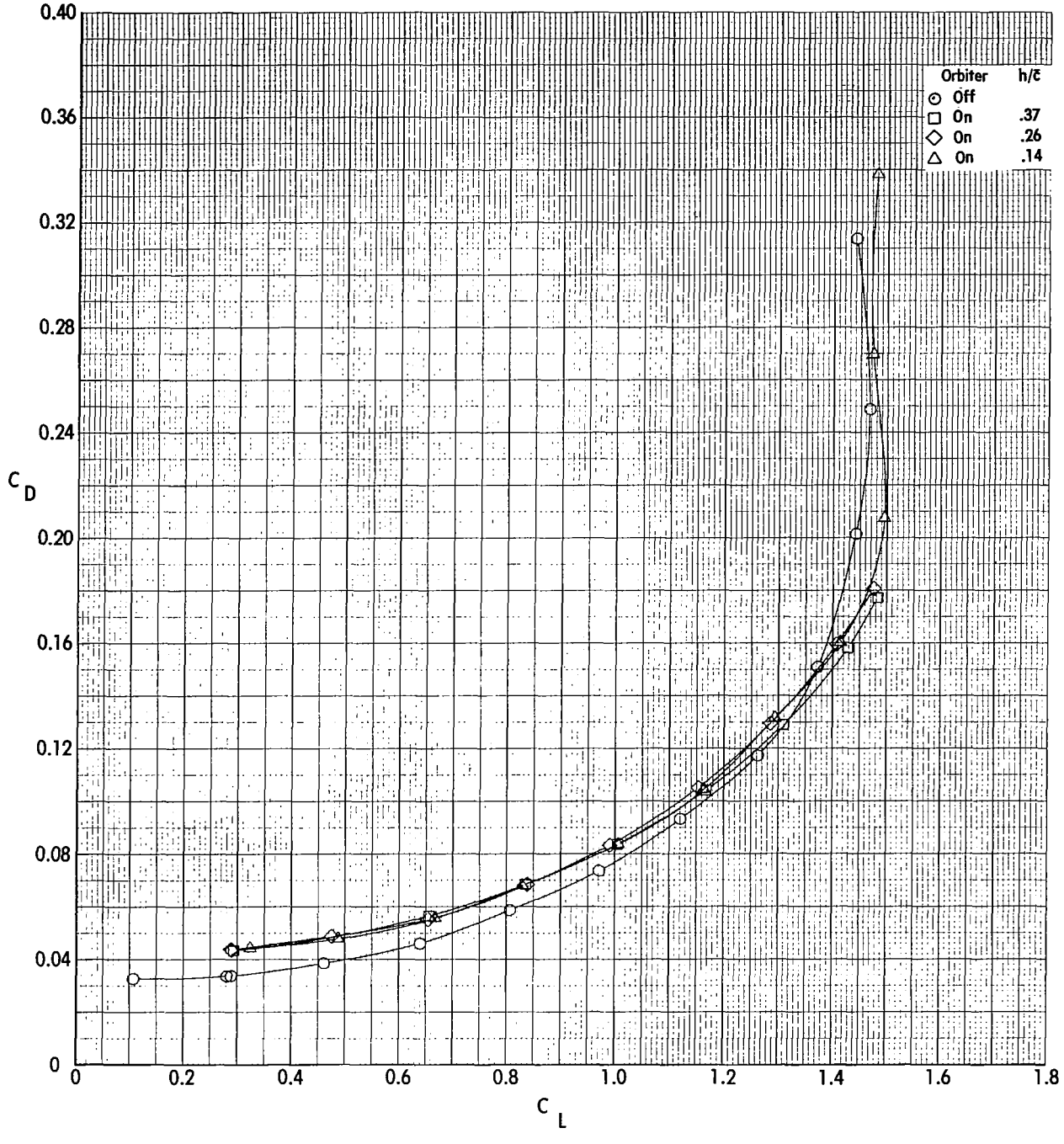

(b) Variation of C_D with C_L.

Figure 14.- Concluded.

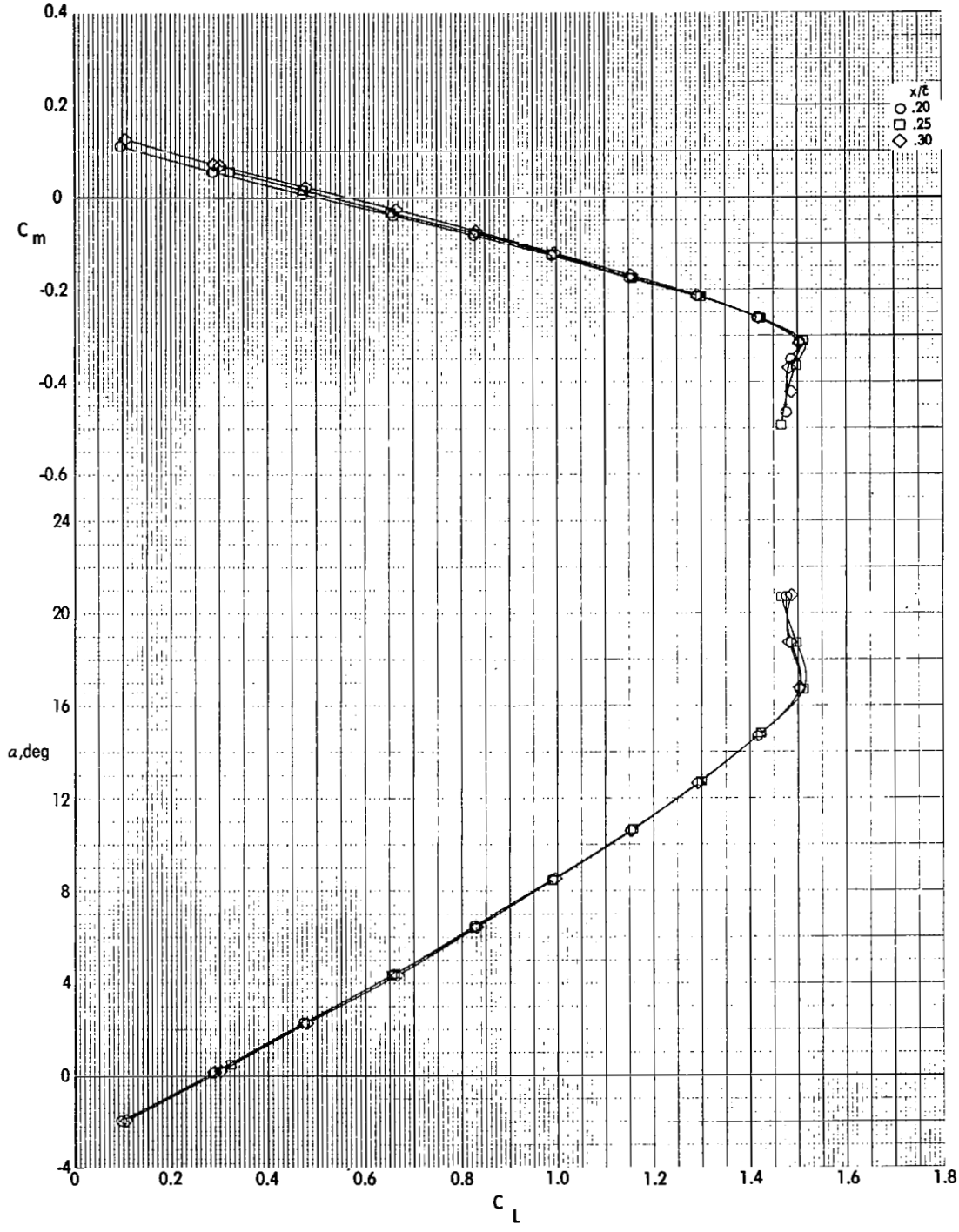

(a) Variation of C_m and α with C_L.

Figure 15.- Longitudinal characteristics of transport model $(i_t = -5^o)$ with orbiter payload with tail fairing $(h/\bar{c} = 0.37)$ at various longitudinal locations.

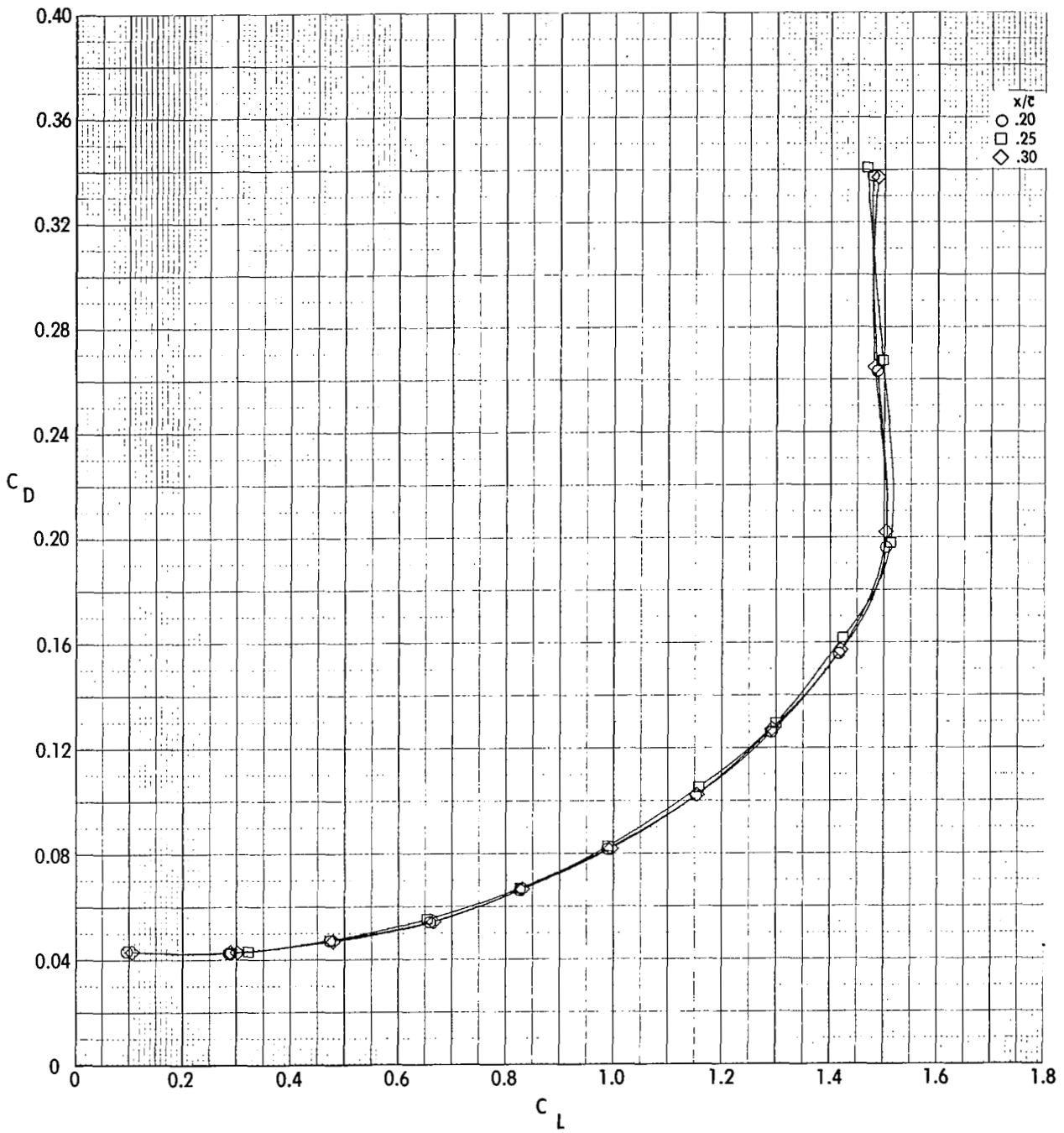

(b) Variation of C_D with C_L.

Figure 15.- Concluded.

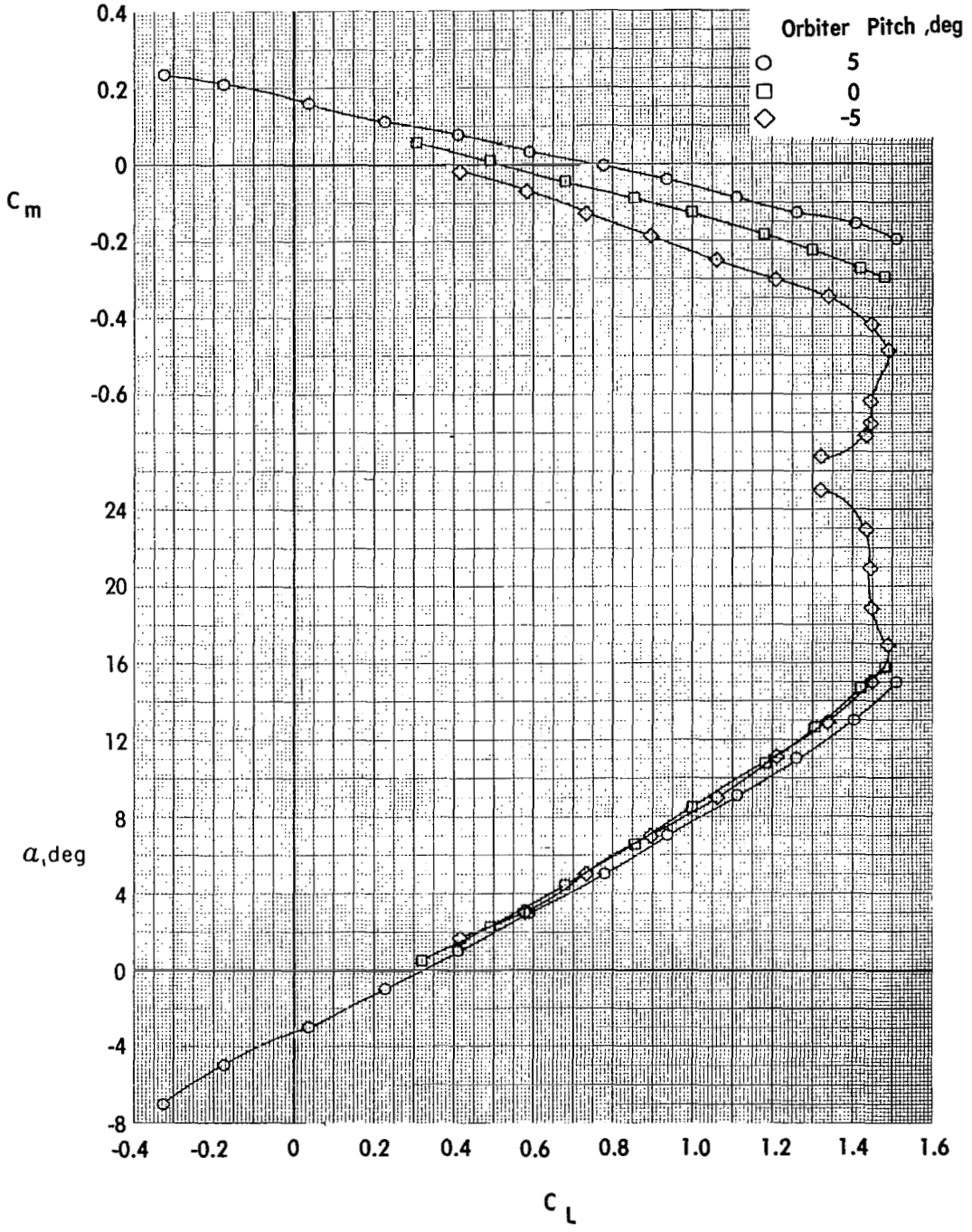

(a) Variation of C_m and α with C_L.

Figure 16.- Longitudinal characteristics of transport model $(i_t = -5^o)$ with orbiter payload with tail fairing $(h/\bar{c} = 0.37)$ at various pitch angles.

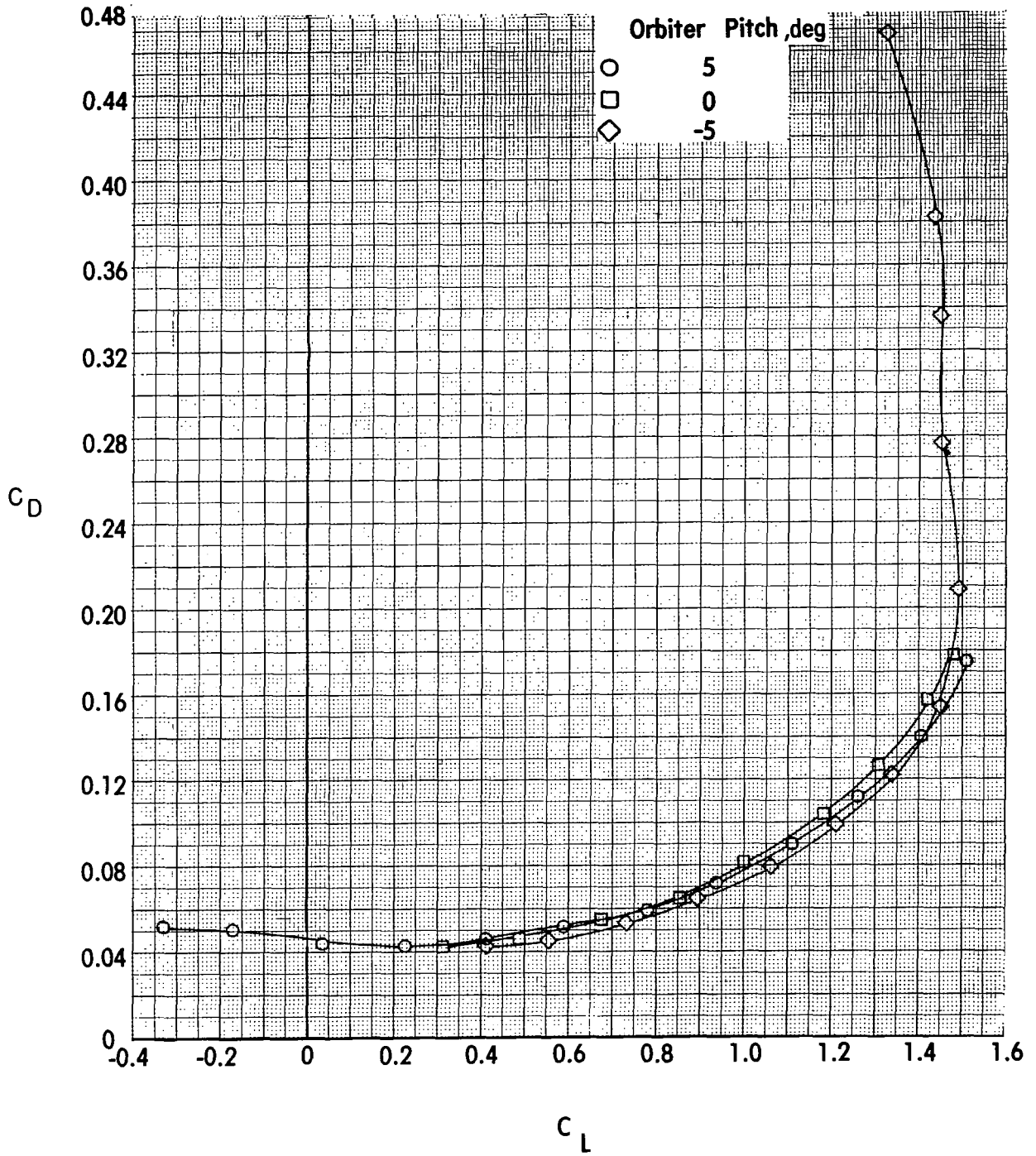

(b) Variation of C_D with C_L.

Figure 16.- Concluded.

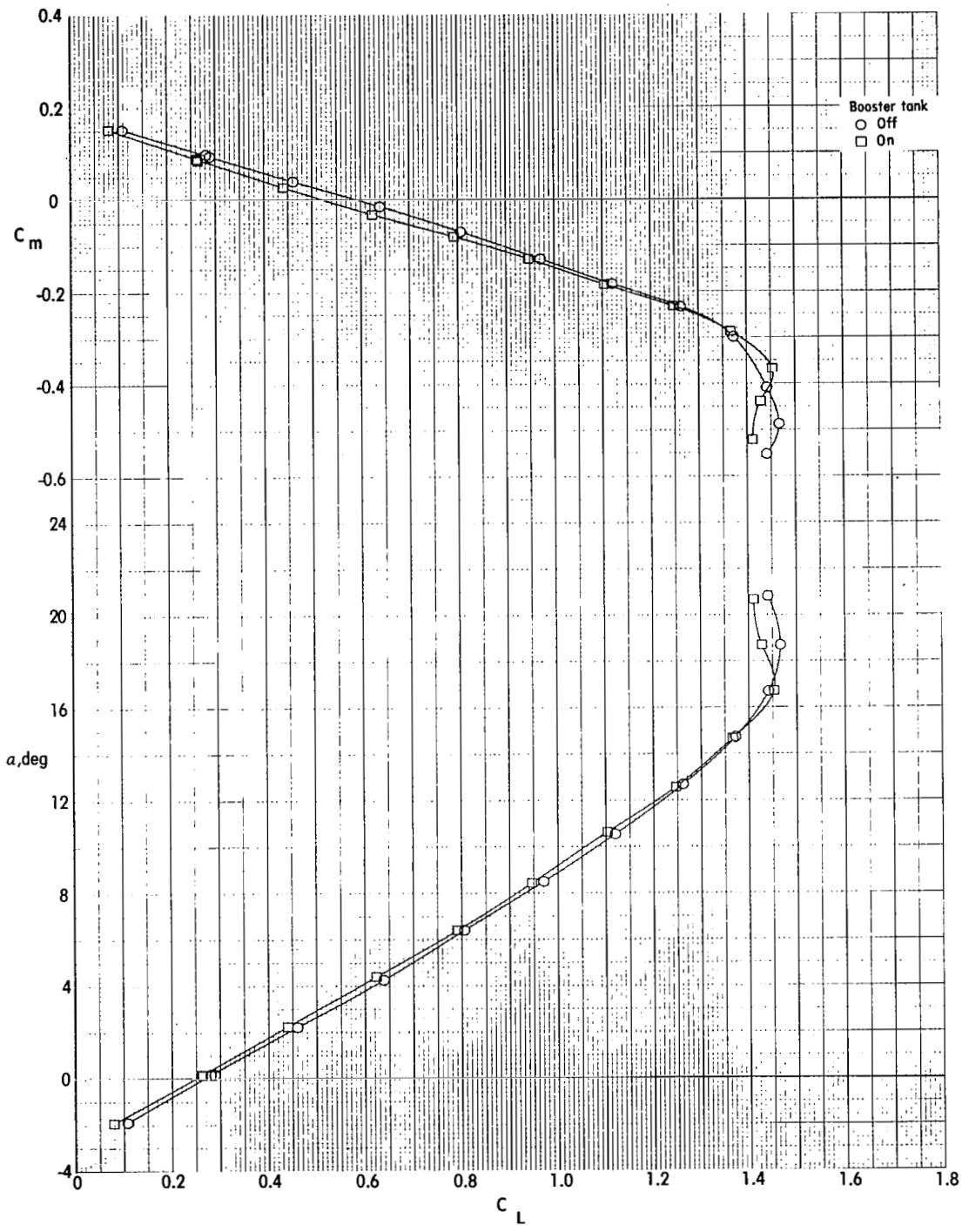

(a) Variation of C_m and α with C_L.

Figure 17.- Longitudinal characteristics of transport model $(i_t = -5^o)$ with booster tank payload. $(x/\bar{c} = 0.25,\ h/\bar{c} = 0.20.)$

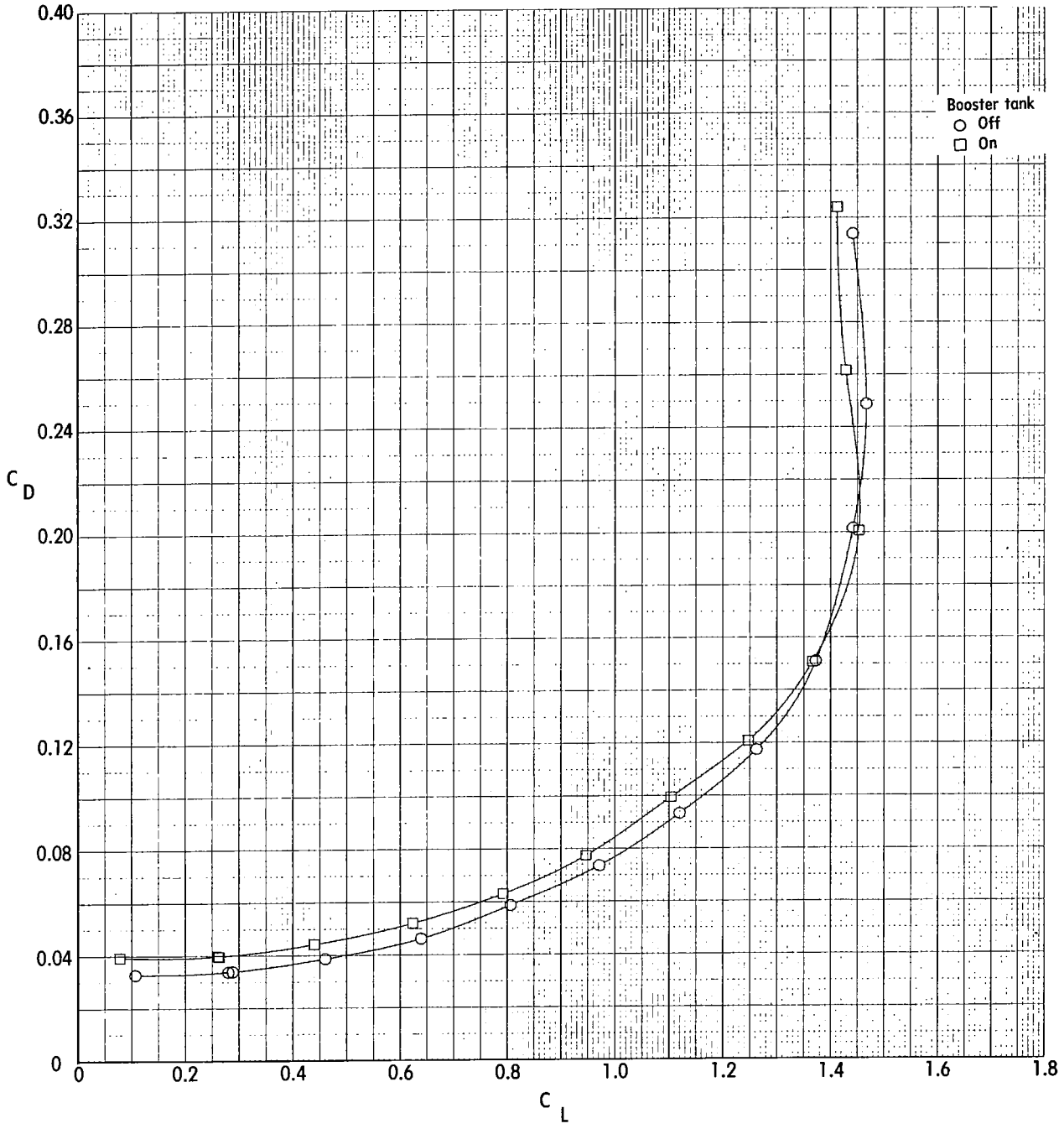

(b) Variation of C_D with C_L.

Figure 17.- Concluded.

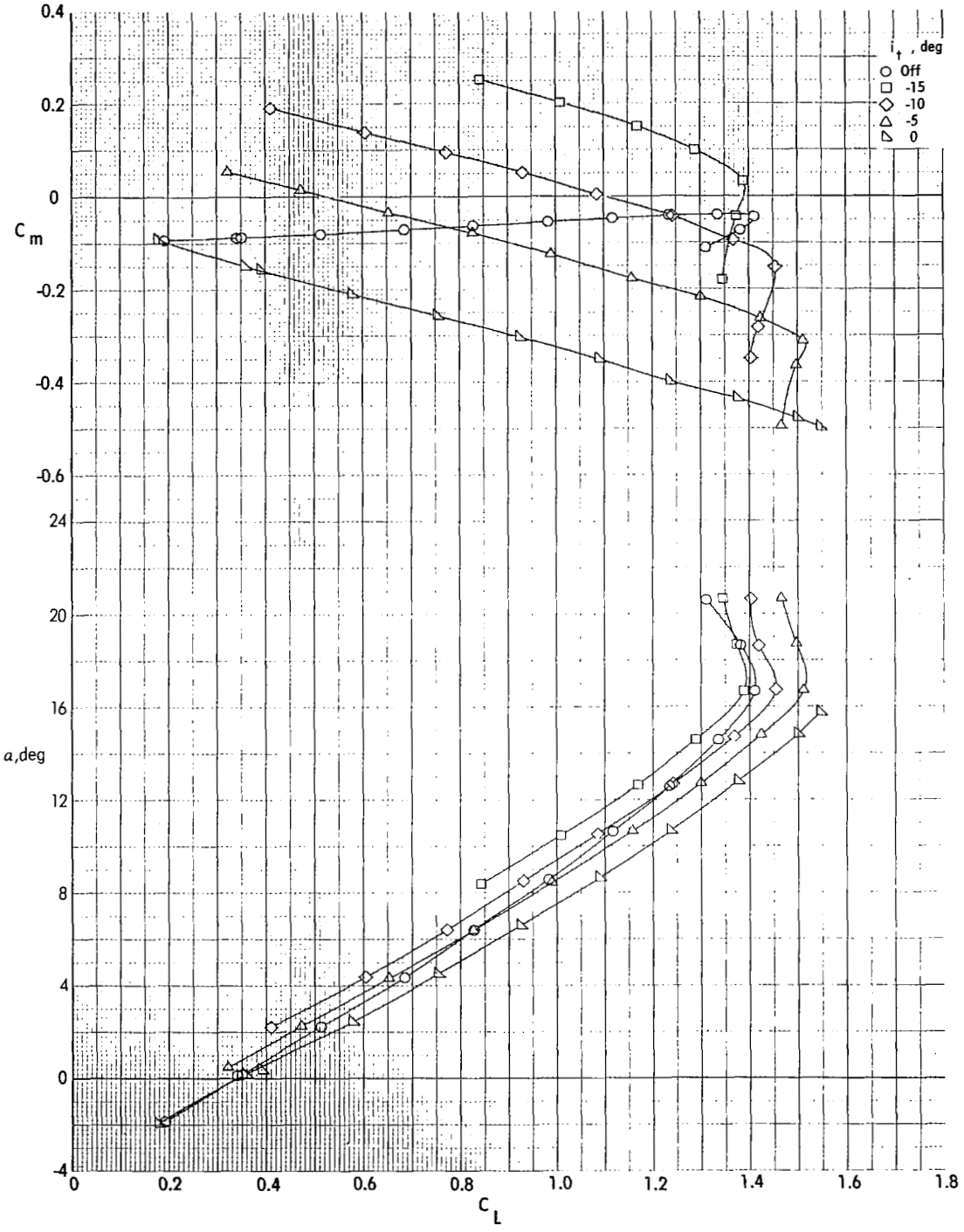

(a) Variation of C_m and α with C_L. ($h/\bar{c}$ = 0.37.)

Figure 18.- Longitudinal control characteristics of transport model with orbiter payload with tail fairing ($x/\bar{c}$ = 0.25).

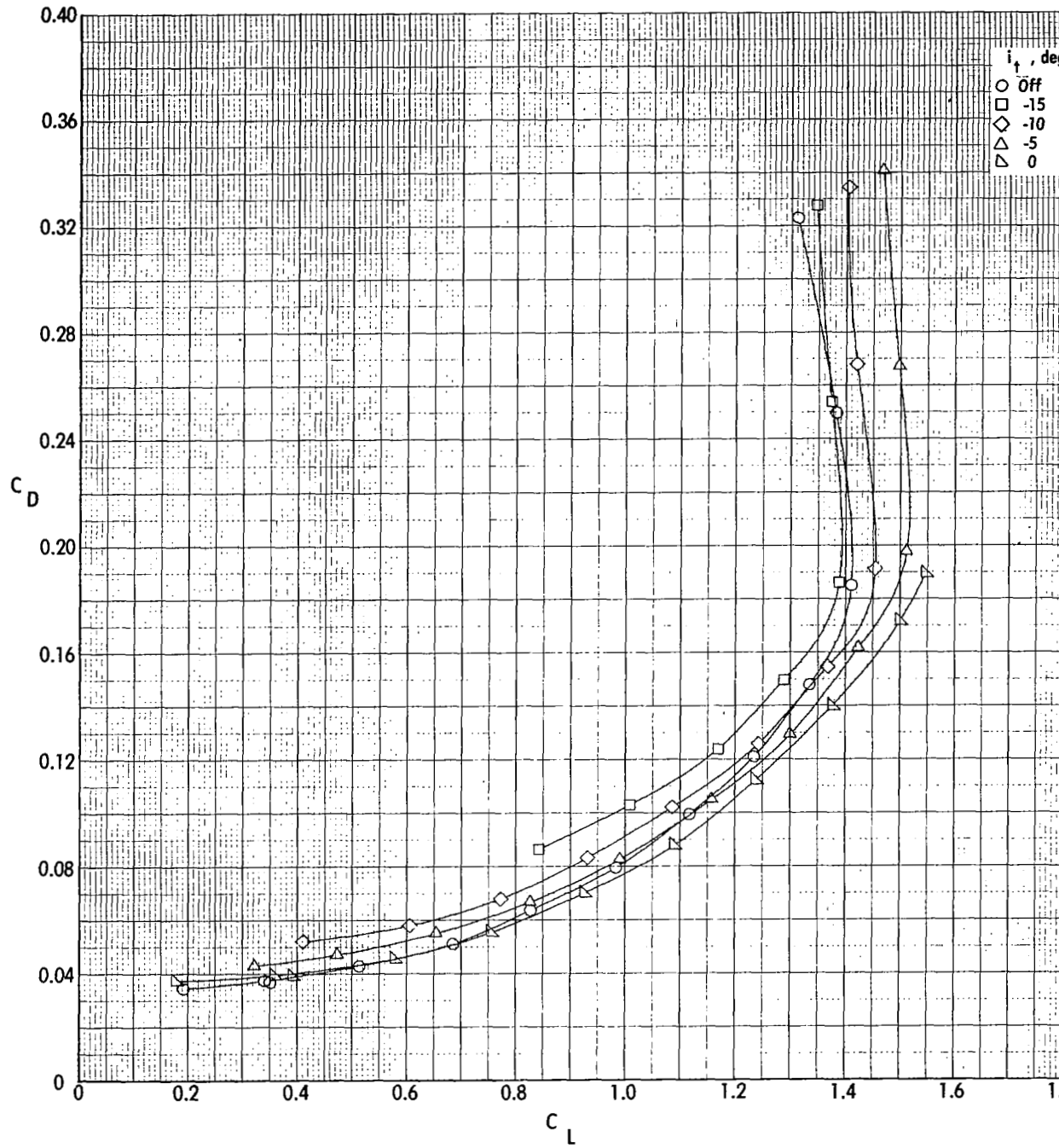

(b) Variation of C_D with C_L. ($h/\bar{c} = 0.37$.)

Figure 18.- Continued.

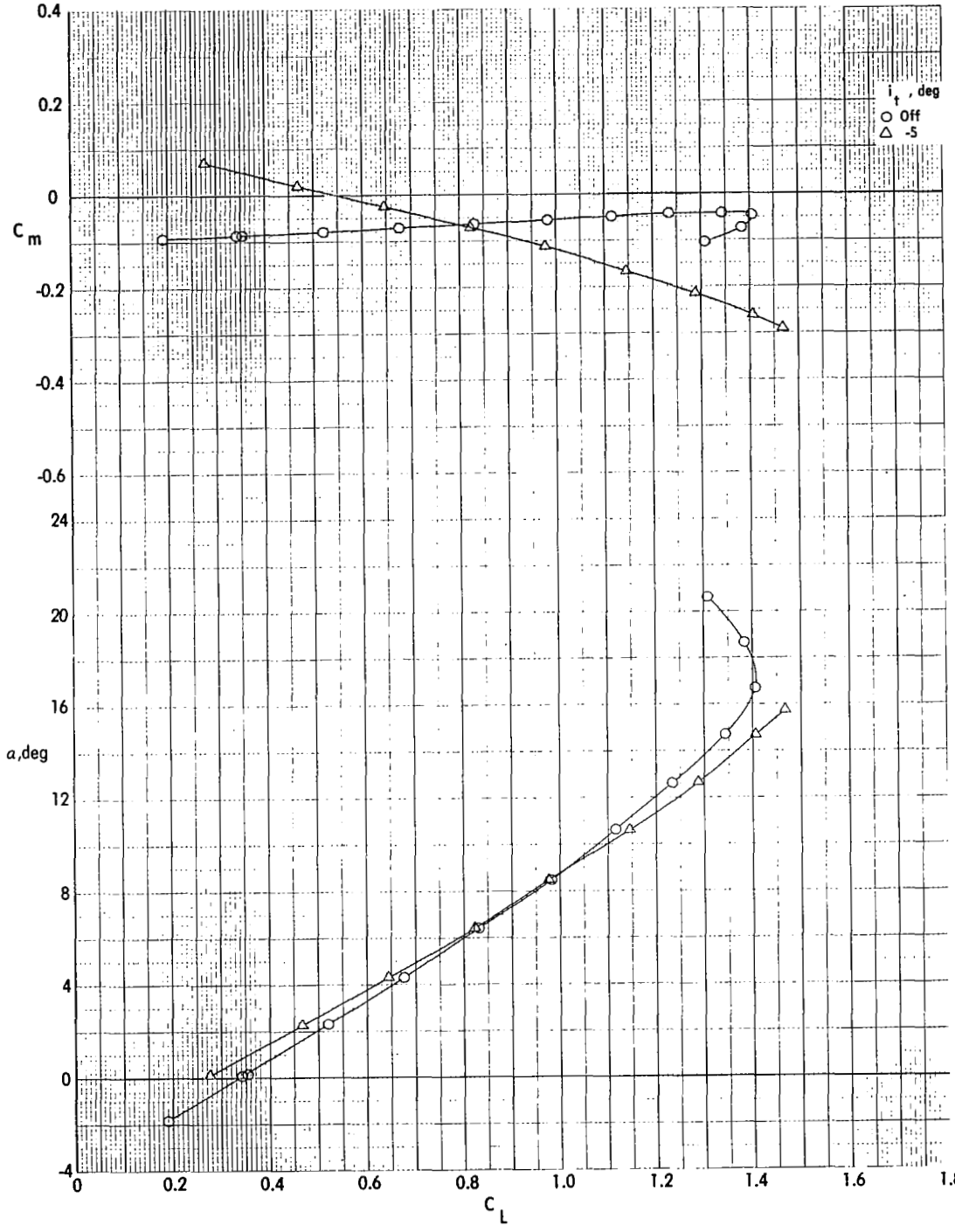

(c) Variation of C_m and α with C_L. ($h/\bar{c} = 0.26$.)

Figure 18.- Continued.

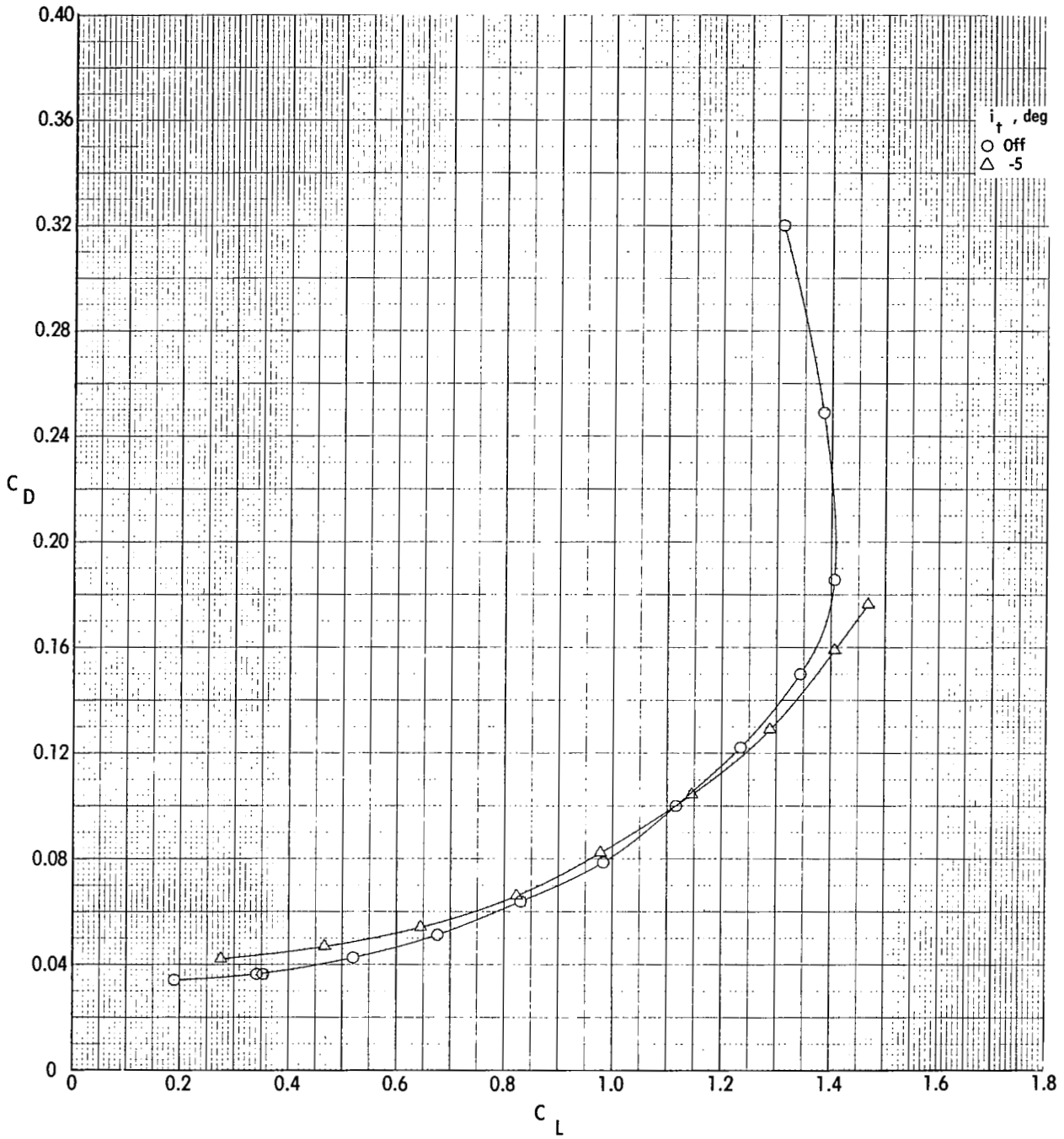

(d) Variation of C_D with C_L. ($h/\bar{c} = 0.26$.)

Figure 18.- Continued.

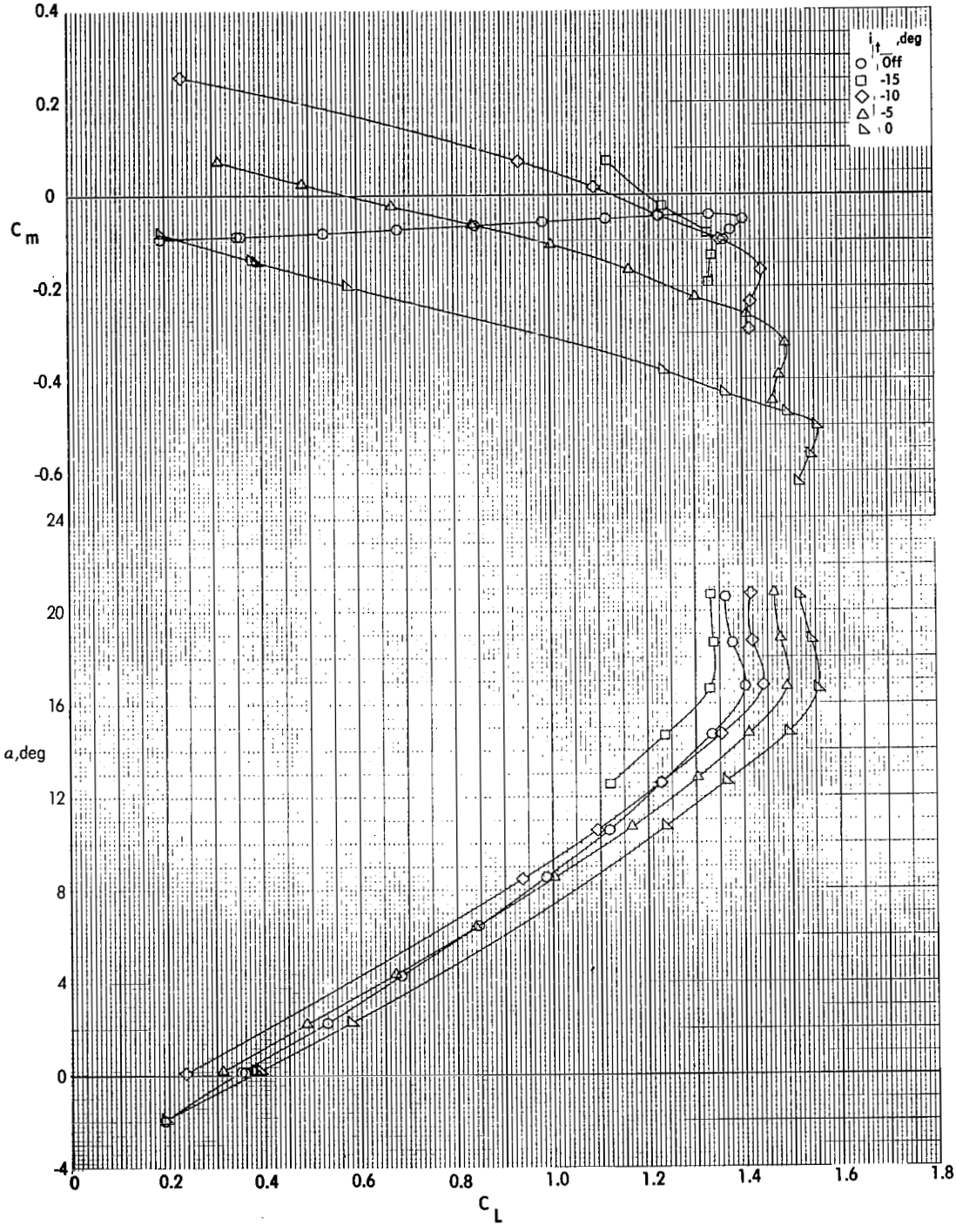

(e) Variation of C_m and α with C_L. ($h/\bar{c} = 0.14$.)

Figure 18.- Continued.

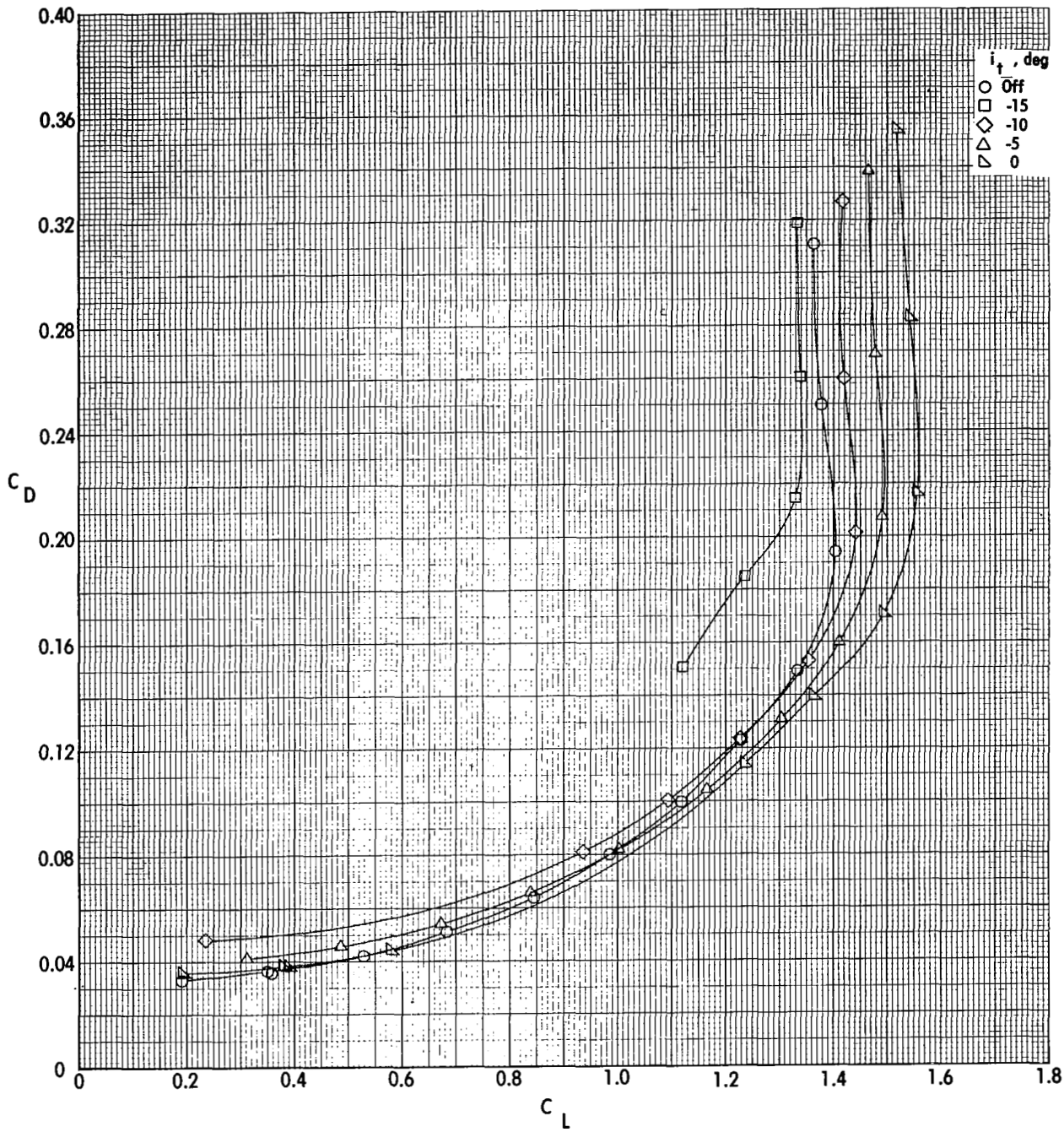

(f) Variation of C_D with C_L. ($h/\bar{c} = 0.14$.)

Figure 18.- Concluded.

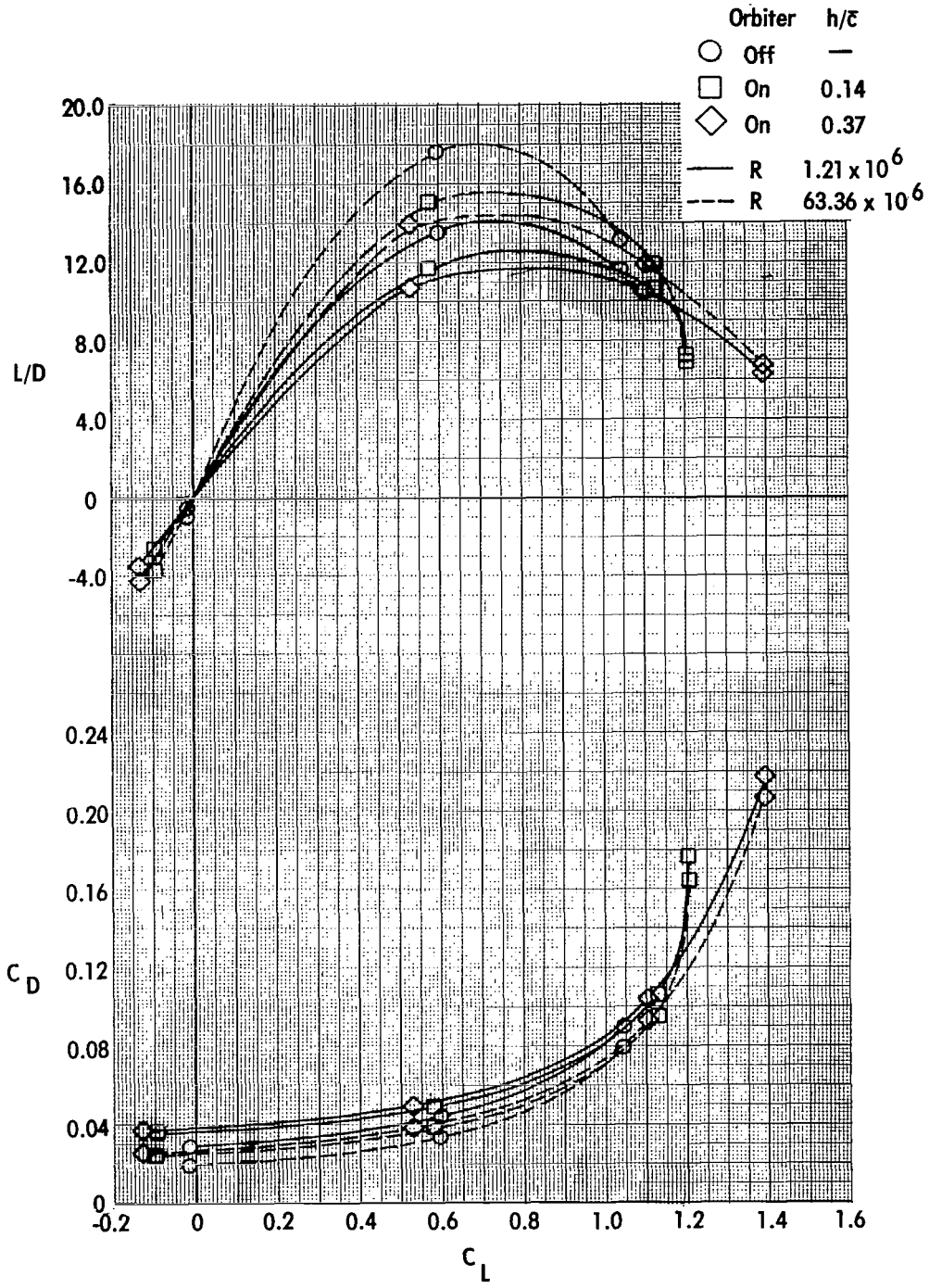

Figure 19.- Trimmed lift-drag ratios and drag polars for several transport configurations at wind-tunnel and full-scale Reynolds numbers.

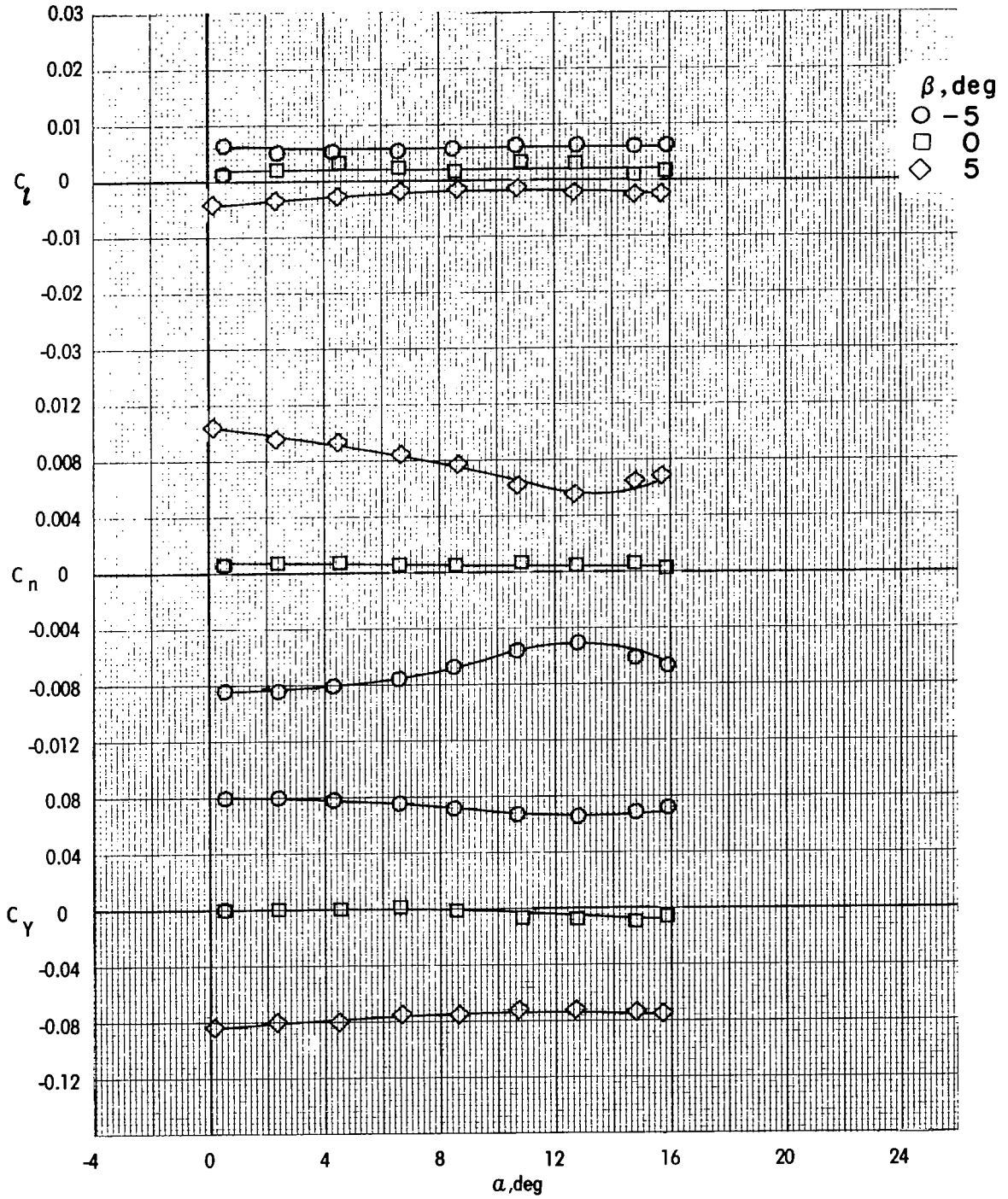

(a) Variation of C_l, C_n, and C_Y with α. ($h/\bar{c} = 0.37$.)

Figure 20.- Lateral-directional characteristics of transport model ($i_t = -5^o$) with orbiter payload with tail fairing ($x/\bar{c} = 0.25$).

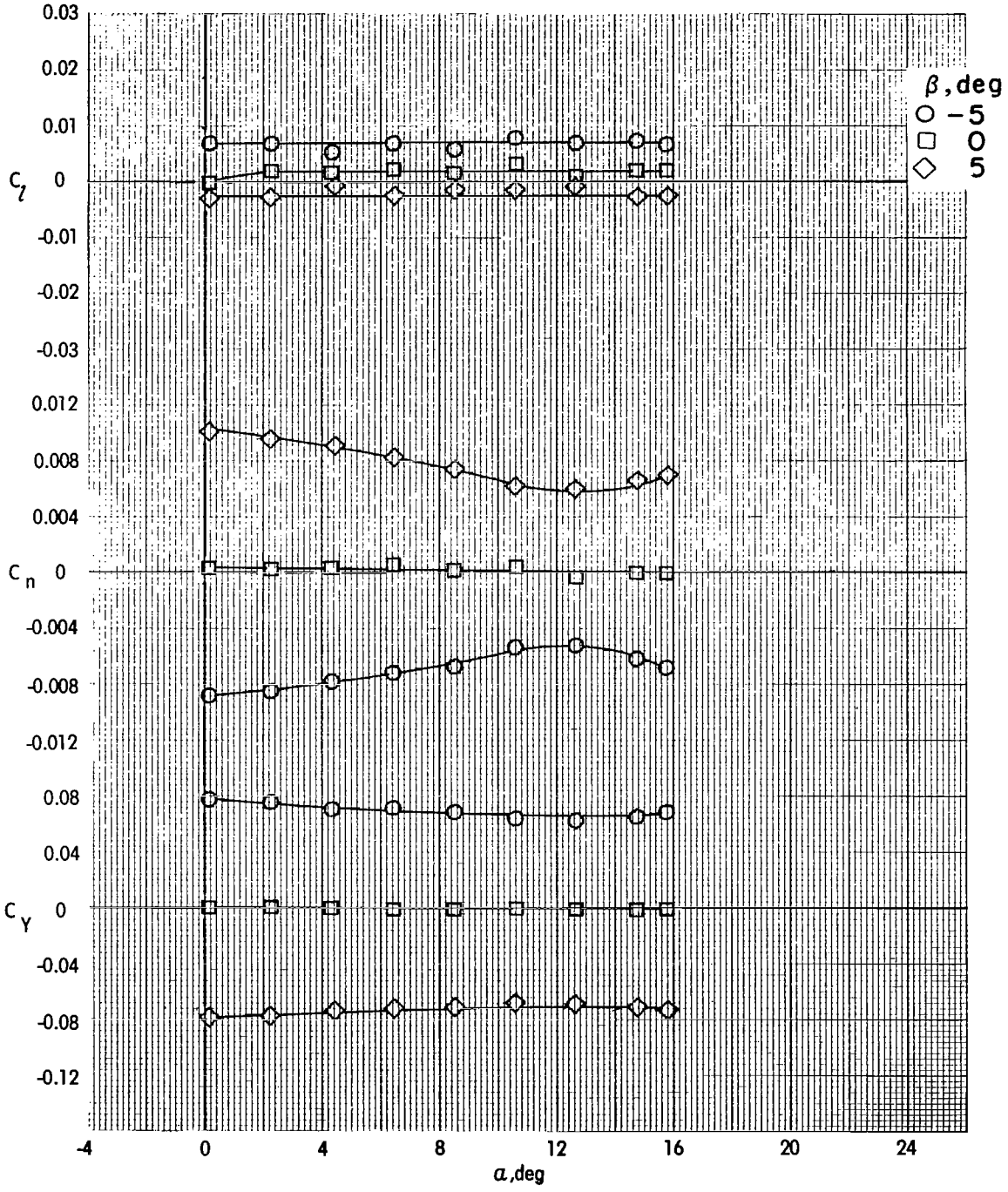

(b) Variation of C_l, C_n, and C_Y with α. ($h/\bar{c} = 0.26$.)

Figure 20.- Continued.

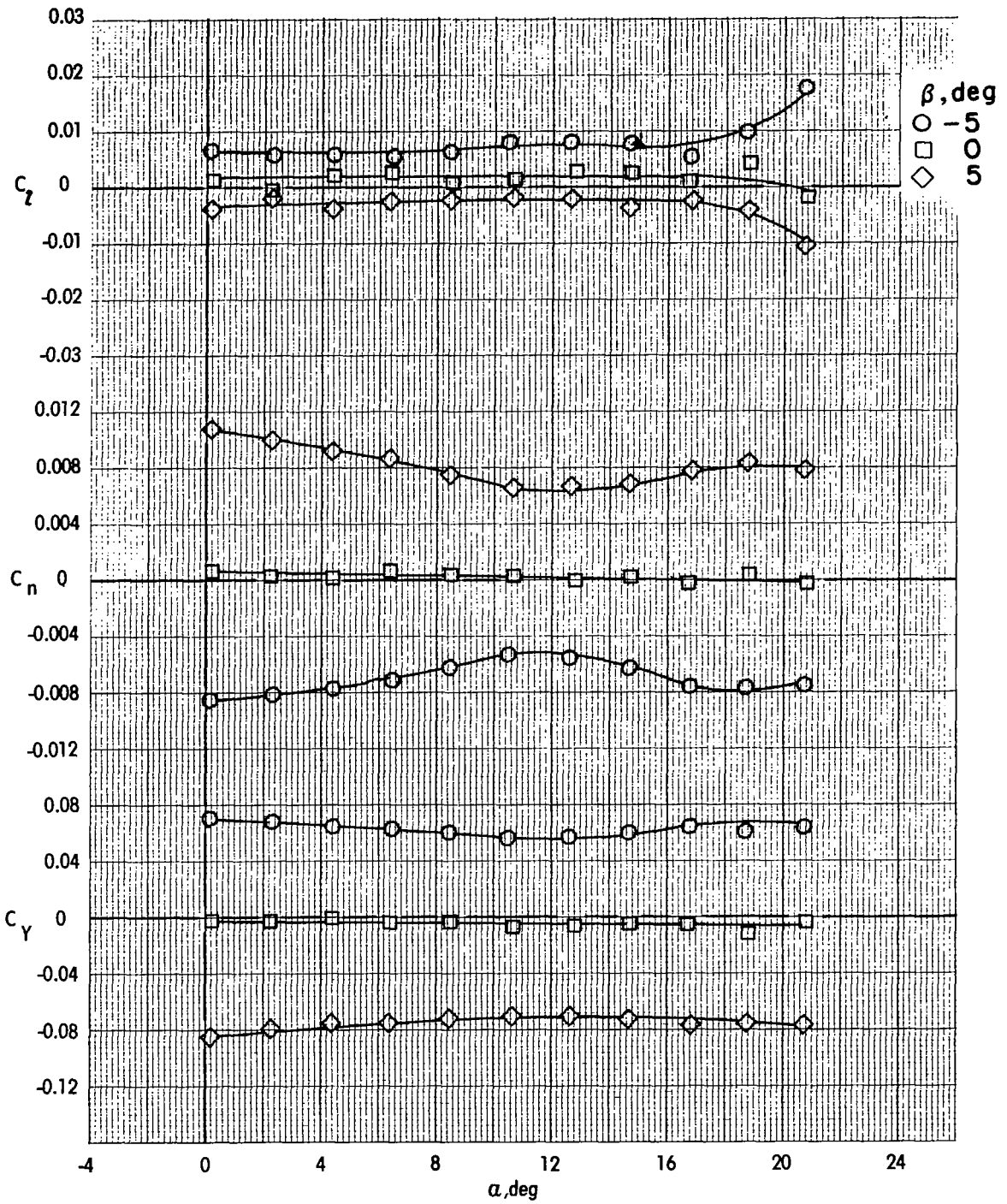

(c) Variation of C_l, C_n, and C_Y with α. ($h/\bar{c} = 0.14$.)

Figure 20.- Concluded.

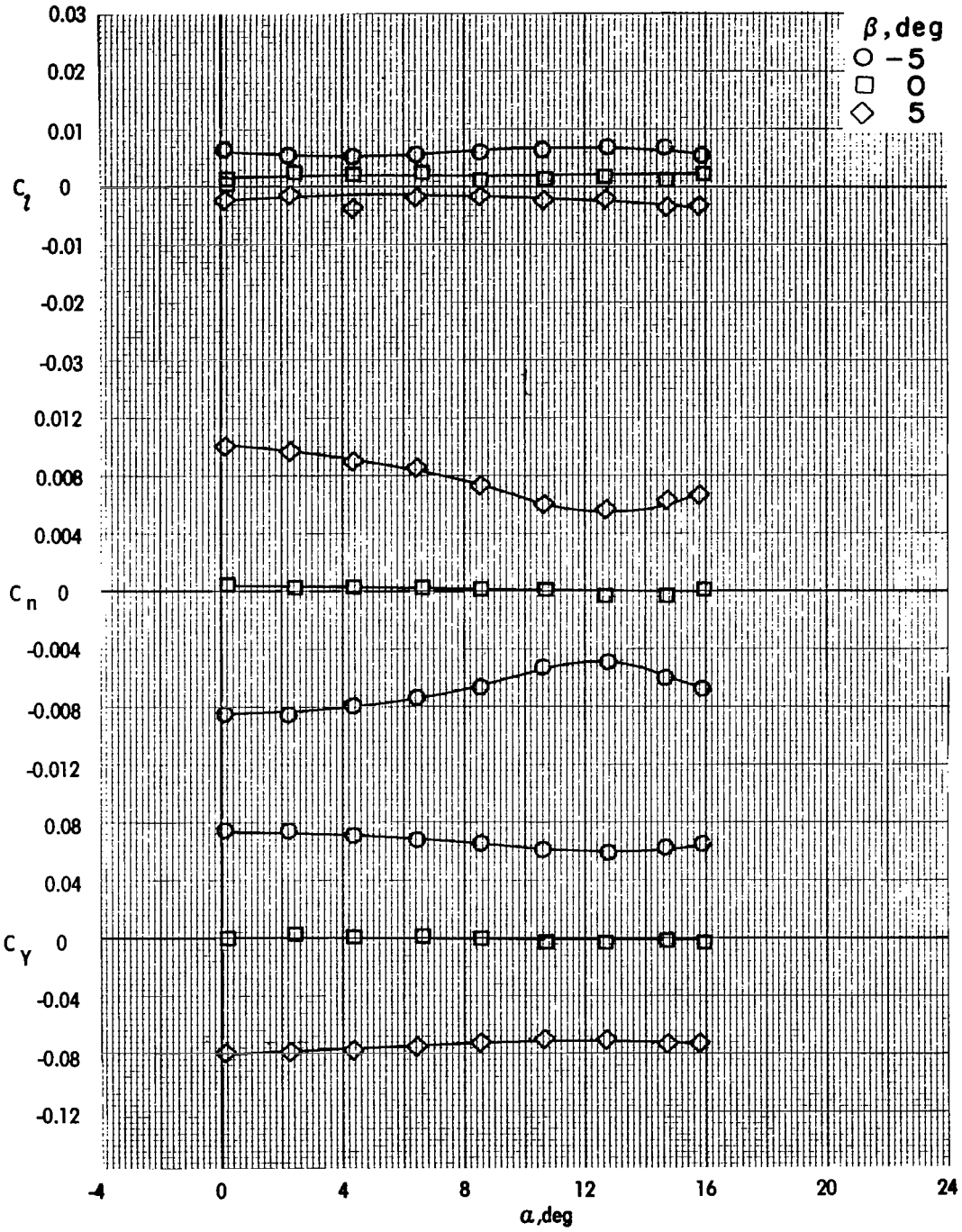

(a) Variation of C_l, C_n, and C_Y with α. ($h/\bar{c} = 0.26$.)

Figure 21.- Lateral-directional characteristics of transport model $(i_t = -5^o)$ with orbiter payload without tail fairing ($x/\bar{c} = 0.25$).

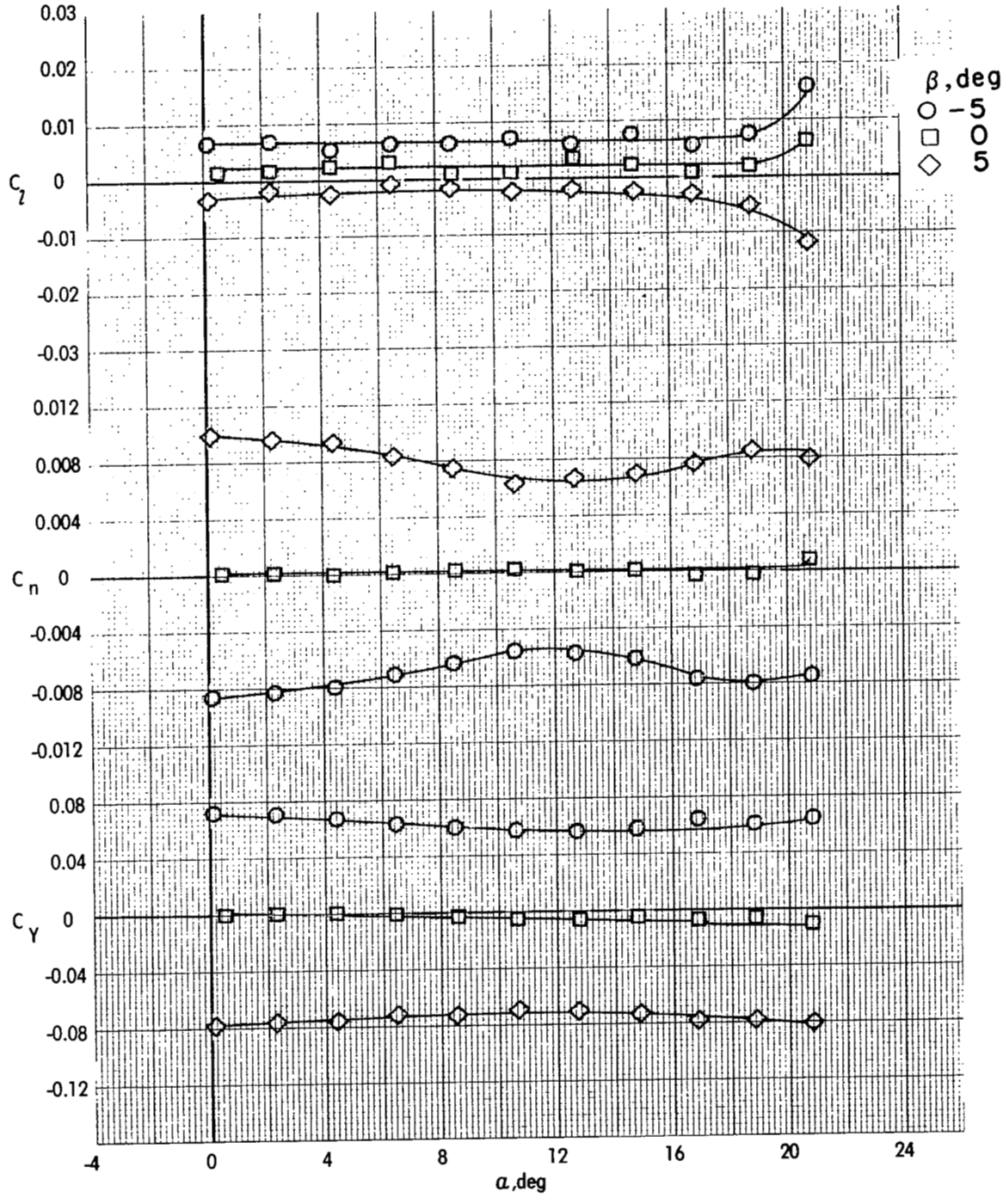

(b) Variation of C_l, C_n, and C_Y with α. ($h/\bar{c} = 0.14$.)

Figure 21.- Concluded.

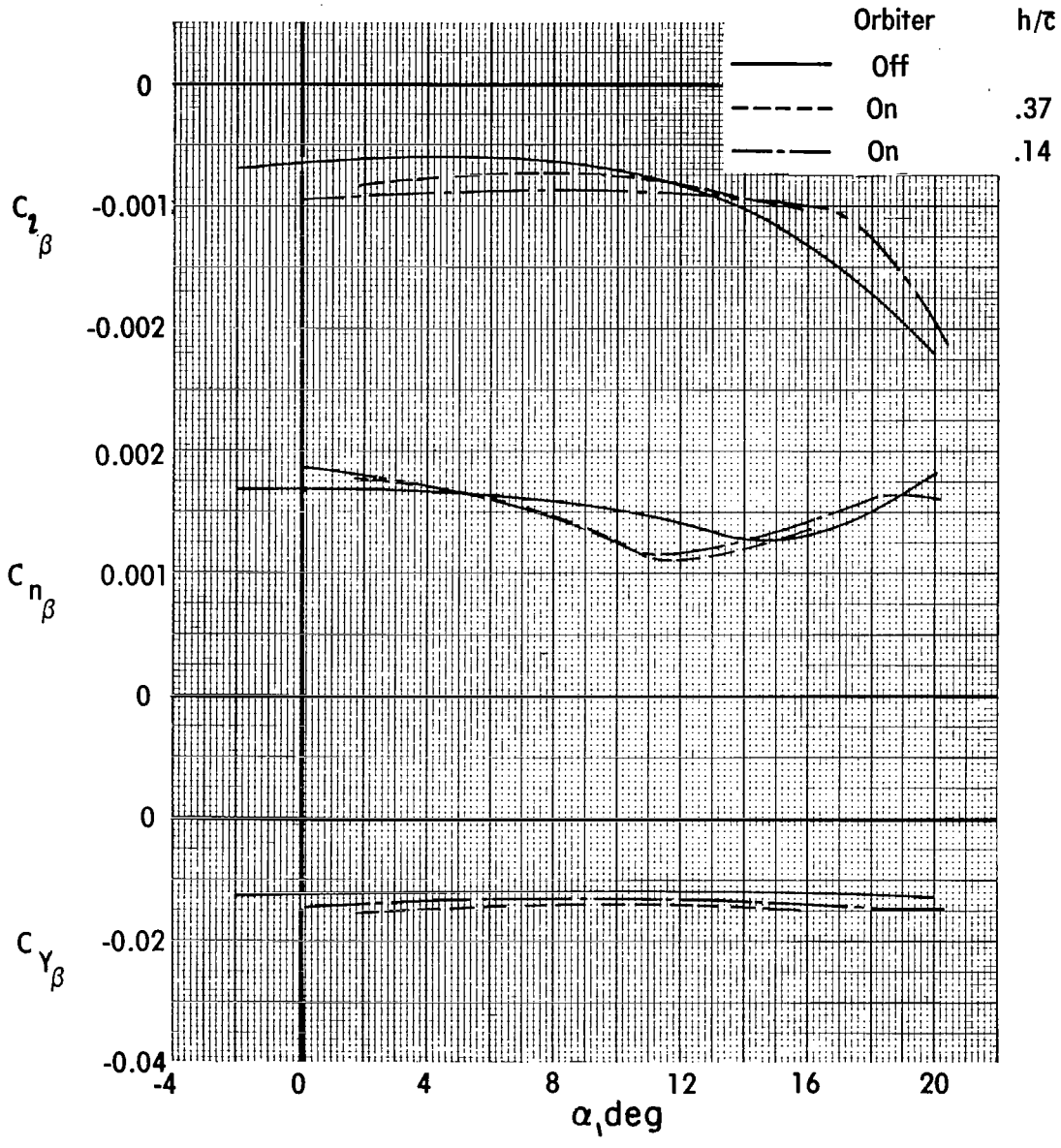

Figure 22.- Lateral-directional stability derivatives for transport model with orbiter payload with tail fairing ($x/\bar{c}$ = 0.25).

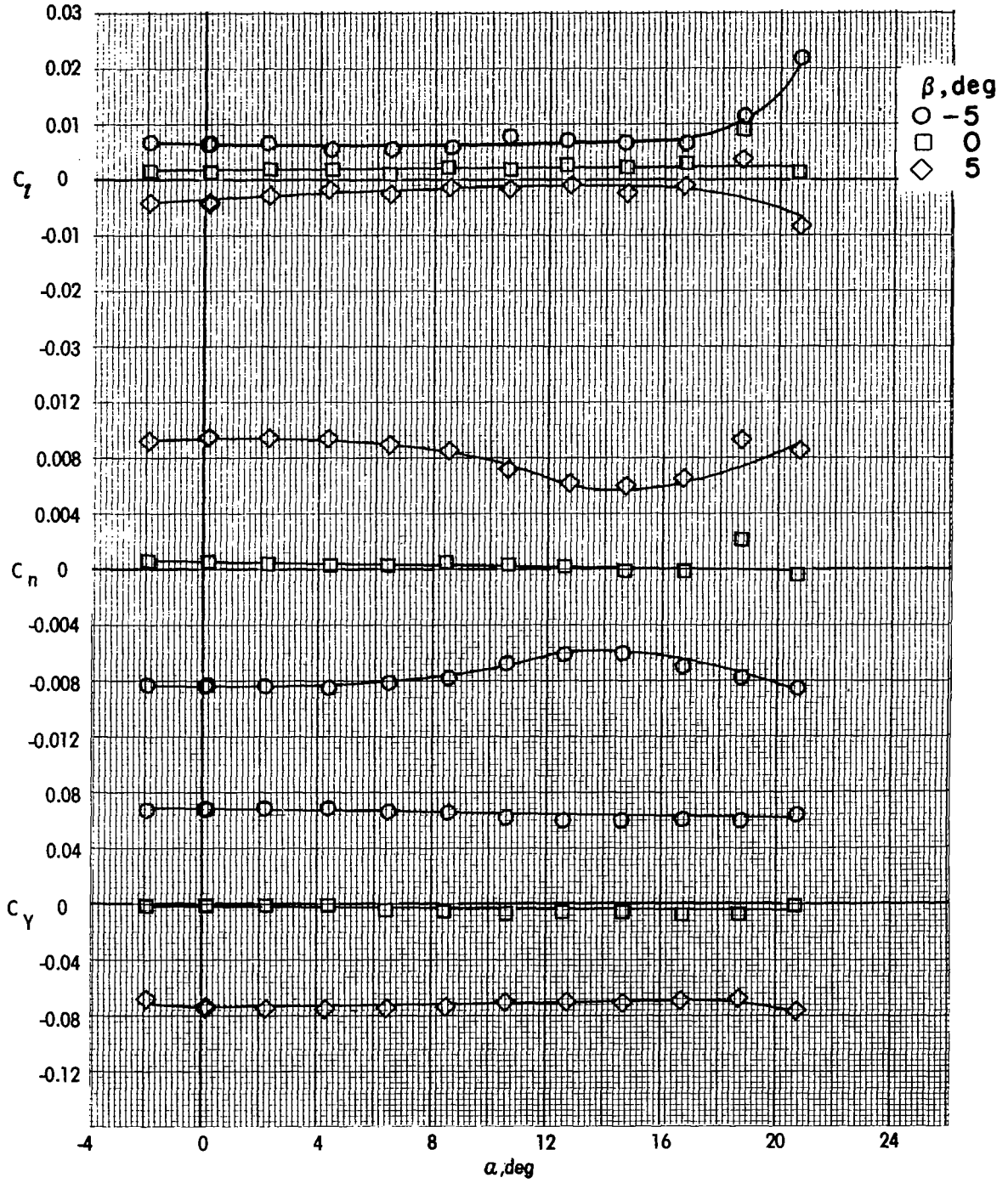

Figure 23.- Lateral-directional characteristics of transport model $\left(i_t = -5^o\right)$ with booster tank payload. $(x/\bar{c} = 0.25; \quad h/\bar{c} = 0.20.)$